HAL open science

Inter-Annual Variability of the Along-Shore Lagrangian Transport Success in the Southern Benguela Current Upwelling System

Moagabo Natalie Ragoasha, Steven Herbette, Jennifer Veitch, Gildas Cambon, Chris J. C. Reason, Claude Roy

To cite this version:

Moagabo Natalie Ragoasha, Steven Herbette, Jennifer Veitch, Gildas Cambon, Chris J. C. Reason, et al.. Inter-Annual Variability of the Along-Shore Lagrangian Transport Success in the Southern Benguela Current Upwelling System. Journal of Geophysical Research. Oceans, 2022, 127, 10.1029/2020JC017114 . insu-03683300

HAL Id: insu-03683300

https://insu.hal.science/insu-03683300v1

Submitted on 16 Mar 2023

HAL is a multi-disciplinary open access archive for the deposit and dissemination of scientific research documents, whether they are published or not. The documents may come from teaching and research institutions in France or abroad, or from public or private research centers.

L'archive ouverte pluridisciplinaire **HAL**, est destinée au dépôt et à la diffusion de documents scientifiques de niveau recherche, publiés ou non, émanant des établissements d'enseignement et de recherche français ou étrangers, des laboratoires publics ou privés.

Distributed under a Creative Commons Attribution - NonCommercial - ShareAlike 4.0 International License

Check for updates

ADVANCING EARTH AND SPACE SCIENCE

JGR Oceans

RESEARCH ARTICLE
10.1029/2020JC017114

Key Points:

- There are multiple physical drivers of the interannual variability of along-shore transport success in the southern Benguela upwelling
- Positive anomalies of transport success are associated with a strong Benguela Jet, reduced offshore and southward transport
- Negative anomalies are associated with enhanced offshore and southward particles transport, and anticyclonic eddies

Correspondence to:
S. Herbette,
steven.herbette@univ-brest.fr

Citation:
Ragoasha, M. N., Herbette, S., Veitch, J., Cambon, G., Reason, C. J. C., & Roy, C. (2022). Inter-annual variability of the along-shore Lagrangian transport success in the southern Benguela Current upwelling system. *Journal of Geophysical Research: Oceans*, *127*, e2020JC017114. https://doi.org/10.1029/2020JC017114

Received 24 DEC 2020
Accepted 13 FEB 2022

The copyright line for this article was changed on 9 JUL 2022 after original online publication.

Author Contributions:
Conceptualization: Moagabo Natalie Ragoasha, Steven Herbette, Claude Roy
Formal analysis: Steven Herbette
Funding acquisition: Moagabo Natalie Ragoasha, Steven Herbette
Investigation: Moagabo Natalie Ragoasha, Steven Herbette, Jennifer Veitch
Methodology: Moagabo Natalie Ragoasha, Steven Herbette, Jennifer Veitch, Gildas Cambon
Project Administration: Steven Herbette, Claude Roy

© 2022. The Authors.
This is an open access article under the terms of the Creative Commons Attribution-NonCommercial-NoDerivs License, which permits use and distribution in any medium, provided the original work is properly cited, the use is non-commercial and no modifications or adaptations are made.

Inter-Annual Variability of the Along-Shore Lagrangian Transport Success in the Southern Benguela Current Upwelling System

Moagabo Natalie Ragoasha[1,2], Steven Herbette[1], Jennifer Veitch[3,4], Gildas Cambon[1], Chris J. C. Reason[2], and Claude Roy[1]

[1]Laboratoire d'Océanographie Physique et Spatiale, IUEM, University Brest - CNRS - IRD - Ifremer, Brest, France, [2]Department of Oceanography, University of Cape Town, Cape Town, South Africa, [3]SAEON, Egagasini Node, Cape Town, South Africa, [4]Department of Oceanography, Nansen-Tutu Centre, Marine Research Institute, University of Cape Town, Cape Town, South Africa

Abstract A 3-km resolution regional ocean model is used to investigate the role of wind-driven coastal circulation and mesoscale variability on the inter-annual variability of transport success in the southern Benguela between Cape Point (34°S) and St Helena Bay (32°S) from 1992 to 2011. Lagrangian particles are released within the top 100 m of the water column along an across-shore transect off Cape Point. Transport success is given by the ratio of the number of particles that reach St Helena Bay over the total number of particles released. The analysis of transport success anomalies and their relationship with the local circulation and wind forcing reveal that there is no single driver of the inter-annual variability. The transport success variability of particles released on the shelf (depths <300 m) mainly depends on their capacity to remain embedded within the coastal Benguela Jet. Nevertheless, peaks in offshore Ekman transport and episodic occurrence of a poleward inner-shelf counter-current contribute to negative anomalies. For particles released on the outer shelf edge (depths >500 m), across-shore transports induced by mesoscale eddies are the main contributors to transport success variability. Rare passage of Agulhas rings near the shelf edge can induce strong offshore advection of particles into the open ocean. In contrast, shelf-edge cyclonic eddies favor the onshore transport of particles originating from the outer shelf edge and thus contribute to increasing transport success.

Plain Language Summary This study investigates the inter-annual variation of Lagrangian transport in the southern Benguela Current upwelling system using a high-resolution regional ocean model and particle tracking experiments. Transport of fish eggs and larvae by upper ocean currents is crucial for the marine ecosystem in this highly productive region since the spawning and nursery areas used by anchovies are separated by large distances (~400 km). The alongshore connectivity between the Cape Peninsula and St Helena Bay from 1992 to 2011 is analyzed and linked to the regional ocean circulation and wind-forcing on an inter-annual time scale. We find that transport success is influenced by several drivers including the Benguela Jet, Ekman transport, the coastal inner-shelf poleward counter-current, and occasional interactions with eddies such as Agulhas rings and shelf-edge cyclonic eddies. These findings provide a valuable information for future studies on the role of the physical drivers that impact the transport of larvae and eggs in the southern Benguela, underlining that no single driver can account solely for extreme positive or negative events in transport success.

1. Introduction

Unlike other eastern boundary upwelling systems (EBUS), the Benguela system off the southwestern coast of Africa is bounded by warm water at both its equatorward and poleward margins. The southern boundary, near 34°–35°S, is in very close proximity to the retroflection region of one of the strongest western boundary current in the global oceans, the Agulhas Current (Figure 1). Large rings of warm water are often shed off this retroflection region and impact on the southern Benguela as well as play an important role in the leakage of heat and salt into the South Atlantic (Beal et al., 2011; Biastoch et al., 2009; de Ruijter et al., 1999; Durgadoo et al., 2013; van Sebille et al., 2009).

As depicted in Figure 1, the Benguela system itself is made up of several components. Offshore from the shelf, the Benguela Ocean Current makes up the eastern limb of the South Atlantic subtropical gyre and is fed by the

21699291, 2022, 3, Downloaded from https://agupubs.onlinelibrary.wiley.com/doi/10.1029/2020JC017114 by Cochrane France, Wiley Online Library on [16/03/2023]. See the Terms and Conditions (https://onlinelibrary.wiley.com/terms-and-conditions) on Wiley Online Library for rules of use; OA articles are governed by the applicable Creative Commons License

Software: Steven Herbette, Gildas Cambon
Supervision: Steven Herbette, Jennifer Veitch, Gildas Cambon, Chris J. C. Reason, Claude Roy
Validation: Steven Herbette, Gildas Cambon
Visualization: Moagabo Natalie Ragoasha, Steven Herbette, Gildas Cambon
Writing – original draft: Moagabo Natalie Ragoasha
Writing – review & editing: Steven Herbette, Jennifer Veitch, Gildas Cambon, Chris J. C. Reason, Claude Roy

South Atlantic Current. Near the shelf edge, the Benguela Jet flows equatorward between Cape Point (34.4°S, 18.5°E) and Cape Columbine (32.8°S, 17.9°E), after which it bifurcates into a shelf jet and an outer-shelf jet. Beneath the Benguela Jet is a poleward flowing under-current lying over the shelf edge, while inshore, there is a poleward flowing counter-current (Nelson, 1989). In summer, the prevailing southerly winds drive coastal upwelling cells at Cape Point and Cape Columbine. The Benguela Jet is driven by the density gradient set up by the cool upwelled water at the coast and the warmer offshore water, which is modulated by warm water associated with Agulhas leakage (Veitch et al., 2017). Upwelling cells north of about 30°S tend to occur throughout the year since the winds remain upwelling favorable. The northern limit of the Benguela system is marked by the Angola-Benguela Frontal Zone near 16°–17°S (Veitch et al., 2006).

The Benguela upwelling system plays an important role in moderating the climate of southwestern Africa and in providing a rich source of nutrients that supports a highly productive marine ecosystem. Small pelagic fisheries have long been exploited by coastal communities in Namibia and western South Africa and there is considerable interest in the maintenance of a sustainable fishing industry. One of the key issues relates to the recruitment of these fish stocks and their interannual variability, which is itself influenced by a set of environmental and biological factors (Bakun, 1996; Painting et al., 1998). Small pelagic fish spawn on the continental shelf, in a non-turbulent environment. Their eggs and larvae are then transported, almost as passive tracers, toward a region of food availability (Parrish et al., 1983). In the southern Benguela upwelling system (SBUS), anchovies spawn from October to March on the Agulhas Bank (Figure 1), located off the south-west and south coast of South Africa (Painting et al., 1998; van der Lingen & Huggett, 2003). These eggs and larvae are then advected northward for about 400 km along the west coast toward the food-rich and retentive nursery area of St Helena Bay (32°S). This transport is facilitated by the Benguela Jet (Bang & Andrews, 1974; Gordon, 1985; Hutchings et al., 1998; Nelson, 1989; Shelton & Hutchings, 1982; Shillington, 1998; Veitch et al., 2017). The larvae that get successfully transported into the nursery area and survive into adults are considered as recruits. Considerable interannual variability in recruitment presents a challenge for fisheries management (Huggett et al., 2003; van der Lingen et al., 2002).

Variability in the passive transport of eggs and larvae, from the spawning ground to the nursery area, has long been considered one of the critical factors influencing stock's recruits (Hutchings, 1992; Hutchings et al., 1998; Shannon et al., 1996). This assumption has since been corroborated by several numerical Lagrangian transport studies, which, at first, were limited to monthly climatological forcing, excluding any externally forced interannual variability (Huggett et al., 2003; Mullon et al., 2003; Parada et al., 2003, 2008). However, the importance of using a realistic, time-varying surface forcing was highlighted by Blanke et al. (2005). Remotely driven ocean processes, such as the southward propagating coastal Kelvin waves (Illig, Bachèlery, et al., 2018), or inter-annual variability of Agulhas leakage, have so far been demonstrated to have minor impacts in the southern Benguela (Loveday et al., 2014).

Offshore mesoscale eddies interacting with the shelf edge have long been thought of affecting the alongshore transport success in the southern Benguela (Hutchings et al., 1998), especially if an offshore Agulhas ring interacts with the shelf edge upwelling front (Duncombe-Rae et al., 1992). Larvae located on the shelf can in fact be entrained offshore, away from the shelf-edge Benguela Jet when an anticyclonic eddy lies south-west of Cape Point (Blanke et al., 2009). Nevertheless, they may also be pushed back inshore toward the Benguela Jet when a cyclonic eddy lies in place of its just mentioned counterpart (Blanke et al., 2009). It has also been proven that the presence of an offshore cyclonic circulation pattern in St Helena Bay provides a retentive environment for the nursery area on the shelf (Penven et al., 2000).

The study of Ragoasha et al. (2019) identifies, on a seasonal time scale, the Lagrangian pathways of the connectivity between Cape Point and St Helena Bay and the local physical processes influencing particles' trajectory. Their results highlight the presence of an inshore and offshore route taken by particles traveling from Cape Point to St Helena Bay. This inshore route had already been identified in Blanke et al. (2009) as the most efficient conveyor transporting particles northward, with relative transfer efficiency peaking at 60% seasonally. Ragoasha et al. (2019) showed that it coincides with particles embedded within the Benguela Jet. Transport success is greatest in spring when the Benguela Jet is characterized by a coherent intensified single-core branch flowing over the 300-m isobath and when moderate wind-induced Ekman transport favors the retention of particles within the jet. At this time of the year, therefore, the optimal pathway leading to successful transport is located inshore of the 300-m isobath (Ragoasha et al., 2019). In summer, during the upwelling season (December–March), transport

21699291, 2022, 3, Downloaded from https://agupubs.onlinelibrary.wiley.com/doi/10.1029/2020JC017114 by Cochrane France, Wiley Online Library on [16/03/2023]. See the Terms and Conditions (https://onlinelibrary.wiley.com/terms-and-conditions) on Wiley Online Library for rules of use; OA articles are governed by the applicable Creative Commons License

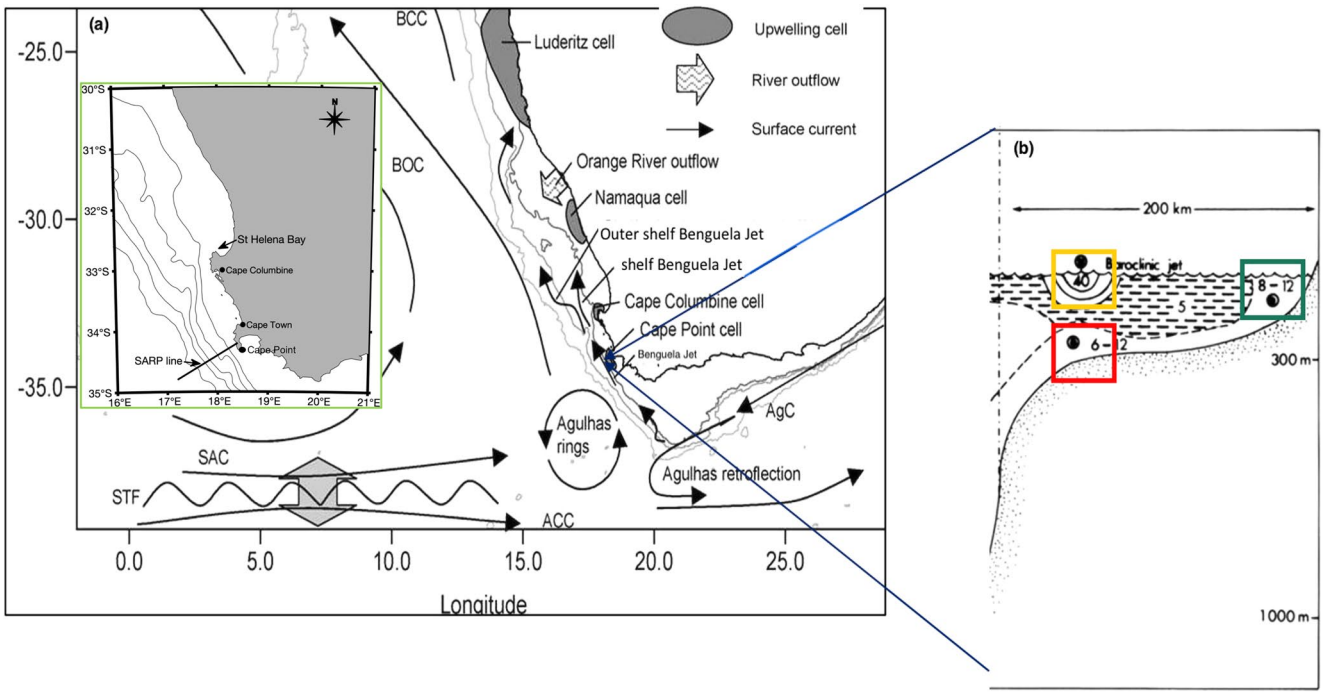

Figure 1. (a) Schematic map of the southern Benguela Current upwelling system showing surface and near-surface currents, frontal zones, major upwelling cells, and bathymetry. Adapted from Hardman-Mountford et al. (2003). ACC: Antarctic Circumpolar Current; AgC: Agulhas Current; BOC: Benguela Oceanic Current; SAC: South Atlantic Current; STF: subtropical front. The insert map shows the locations of St Helena Bay nursery area, and the across-shelf SARP line*, just north of Cape Point. (b) Vertical schematic picture of along-shore currents on an across-shore transect off Cape Point based on measurements from Acoustic Doppler Current Profilers (ADCP). Note the presence of the Benguela Jet (yellow box), the shelf-edge poleward under-current (red box), and the inner-shelf poleward counter-current (green box). Adapted from Nelson (1989). *The South African Sardine and Anchovy Recruitment Program (SARP) line is an across-shore section off Cape Point (34°S) used to assess the transport success of sardine and anchovy eggs and larvae (Fowler & Boyd, 1998; Hampton, 1996).

success becomes less efficient, and the inshore route no longer dominates, as the majority of particles follow offshore pathways (Ragoasha et al., 2019). The Benguela Jet shifts offshore and splits into several branches due to the shoaling of the poleward undercurrent (Ragoasha et al., 2019). The entrainment of particles within the offshore branch of the jet is favored by the dominating offshore wind-induced Ekman transport. Particles trapped in the offshore branch get exposed to higher mesoscale variability and their northward progression is slower than during spring (Ragoasha et al., 2019). While the study of Ragoasha et al. (2019) provides insight into the role of the Benguela Jet, offshore Ekman drift, and mesoscale eddies and their seasonally varying influences on the successful transport of particles, it relied on a relatively coarse horizontal resolution (≃7 km) model which was unable to capture finer scale coastal dynamics, such as the presence of an inner-shelf poleward counter-current (Nelson, 1989) and smaller size (≃30 km) shelf-edge cyclonic eddies originating from the instabilities of the Benguela Jet (Hall & Lutjeharms, 2011; Rubio et al., 2009). Nevertheless, the latter are thought to also impact connectivity (Shannon et al., 1996).

This study is a direct follow-up of the work of Ragoasha et al. (2019) and investigates how local dynamical processes impact the interannual variability of the alongshore connectivity between Cape Point and St Helena Bay. Aside from being forced with an interannually varying atmosphere, it also has a higher resolution horizontal grid (3 km), allowing for a better representation of fine-scale dynamics that impact the transport of particles.

2. Materials and Methods

Our methodology is similar to the one used by Ragoasha et al. (2019): the inter-annual variability of transport success was investigated from 1992 to 2011 using Lagrangian experiments ran using an off-line tracking algorithm called Pyticles (Gula et al., 2014) fed with 20 years of daily three-dimensional velocity fields derived from an inter-annual numerical simulation of the oceanic circulation. However, the model simulation is now based

21699291, 2022, 3, Downloaded from https://agupubs.onlinelibrary.wiley.com/doi/10.1029/2020JC017114 by Cochrane France, Wiley Online Library on [16/03/2023]. See the Terms and Conditions (https://onlinelibrary.wiley.com/terms-and-conditions) on Wiley Online Library for rules of use; OA articles are governed by the applicable Creative Commons License

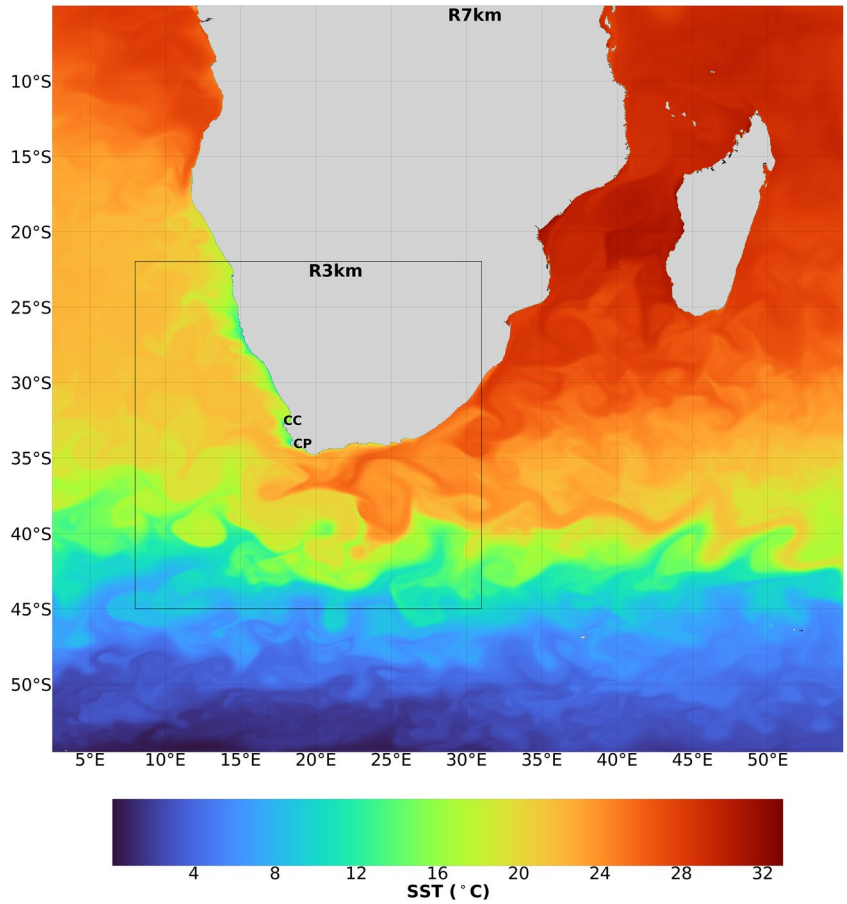

Figure 2. Snapshot of model SST (2005, January, first). The black box delineates the boundaries of the nested 3-km child grid. Within the box, the SST of the 3 km simulation is superimposed upon the one of the 7-km simulation. CP: Cape Point (34°S); CC: Cape Columbine (33°S).

on a higher resolution 3-km nested grid that allows for the first time the impacts of fine-scale dynamics of the Benguela Upwelling System to be investigated.

2.1. The 3-km Model Simulation

This new simulation was run with an off-line and one-way nested approach consisting of a 3-km child grid embedded in a 7-km parent grid (Figure 2). The lower resolution parent simulation (R7KM) supplies boundary conditions to the higher resolution child simulation (R3KM). Boundary conditions are prepared using the roms-2roms algorithm (Mason et al., 2010). The parent simulation is fully described in Ragoasha et al. (2019). The bottom topography for the child grids was also extracted from the Shuttle Radar Topography Mission (SRTM 30 plus) data set (available at http://topex.ucsd.edu/www.html/srtm30.plus.html), subsequently interpolated on the higher resolution grid, and then smoothed similarly to the parent simulation. The same 6-hourly atmospheric forcing (heat, fresh, and momentum fluxes) provided by the CFSR atmospheric reanalysis at 0.3° horizontal resolution (Saha, 2010) were used to compute the surface boundary conditions of the higher resolution simulation. Daily averaged prognostic output variables (u, v, η, T, S) from the parent model were used to specify the ocean currents, sea-surface elevation, temperature, and salinity at the lateral boundaries of the 3-km resolution simulation.

The 3-km simulation was initialized on January 1, 1990 after interpolating the daily average archive of the 7-km simulation on the 3-km grid. The simulation was run from 1990 to 2011 and daily averages of all variables of interest were archived. Our analysis focuses on the 1992–2011 period, as the first 2 years were considered as a spin-up period after which the model had reached a statistical equilibrium.

21699291, 2022, 3, Downloaded from https://agupubs.onlinelibrary.wiley.com/doi/10.1029/2020JC017114 by Cochrane France, Wiley Online Library on [16/03/2023]. See the Terms and Conditions (https://onlinelibrary.wiley.com/terms-and-conditions) on Wiley Online Library for rules of use; OA articles are governed by the applicable Creative Commons License

2.2. Evaluation of the Model's Realism

The model-observation comparison for the child simulation showed that the model could reproduce the average large scale and coastal patterns of the circulation on a seasonal time scale (Figures 3–5).

The high off-shore levels of eddy kinetic energy (EKE), delineated by the 450 $cm^2\ s^{-2}$ EKE contour, are similar in the model and the observations (Figure 3). These high levels are found south-west of Cape Point and extend north-westward. They correspond to the presence of intense mesoscale coherent features that form during the Agulhas Current retroflection and then propagate westward into the South-East Atlantic (Loveday et al., 2014).

The coastal circulation also compares well with observations despite temperature biases at depth (Figures 4 and 5). The northward along-shore Benguela Jet is still present with average velocities approaching 0.2 m s^{-1} (Figure 4). Nevertheless, it now has a much more limited offshore extension and remains located on the shelf edge. One of the most remarkable gain of the 3-km resolution comes from its ability to capture an inner-shelf poleward counter-current on the inshore side of the Benguela Jet (Figure 5), a non-existent feature in the lower resolution simulations of both Veitch et al. (2017) and Ragoasha et al. (2019). This southward flow reaches 0.05 m s^{-1}, which is consistent with the in-situ measurements of Nelson (1989). It is strongest in austral summer and weakest in spring (not shown).

The inshore turbulence is less energetic and can be related to the instabilities of the coastal jets (Veitch et al., 2017) and the presence of coastal trapped waves (Illig, Cadier, et al., 2018; Figure 3). Over the 200–2,000 m isobaths, the model exhibits higher EKE values than the altimetry data, possibly because its higher resolution allows a more accurate representation of the shelf-slope ocean dynamics. In particular, shelf-edge cyclonic eddies, visible on fine resolution AVHRR images but too small to be captured by altimetry, are observed in the model. Pockets of large EKE values tend to be localized in the lee of Cape Point and Cape Columbine during summer and autumn (Figure 3).

2.3. Lagrangian Particle-Tracking Experimental Setup

Particles were randomly released every 12 hr from 1992 to 2011 along the SARP line (Figure 6a), over the upper 100 m of the water column (Figure 6b). The particles were released over 108 defined vertical profiles distributed every 3 km in horizontal distance, with a density of 1.125 particles per meter which resulted in a total of 4,840 particles for each release event. Particles were then followed for 30 days, a time chosen to be much larger than the average traveling time (Ragoasha et al., 2019). For each release event e, transport success $TS_e = \frac{n_e}{4840}$ is given by the ratio of the number of particles reaching St Helena Bay (n_e) over the total number of particles released (4,840).

3. Inter-Annual Variability of Transport Success Anomalies

Ragoasha et al. (2019) already showed that, on a seasonal time scale, the successful transport from the Agulhas Bank to the west coast upwelling region could not only be attributed to a simple wind-induced modulation of the Benguela Jet, but rather a combination of the latter with offshore Ekman transport and off-shelf mesoscale turbulence. The following subsection investigates statistically, on an inter-annual time scale, the link between anomalies of transport success and the local physical processes at play. Correlations between the strength of the Benguela Jet, the alongshore wind stress, the inner-shelf poleward counter-current, the off-shelf EKE, and transport success are first investigated separately.

3.1. Interannual Time Series and Correlations

For each field of interest, the R3km eulerian simulation and the Lagrangian tracking experiment provide us with an inter-annual time series of 6,940 daily average values over the 20 years (1992–2011) period of interest: $I(id)$, with I a generic name standing for either transport success or any of the chosen key dynamical indicator, and id a daily time index. Daily average values are then either average monthly or seasonally. Standardized monthly and seasonal anomalies are then computed to visualize (Figure 7) or correlate the time series, respectively. The three steps of procedure are summarized below:

1. Four inter-annual time series of seasonally average values are built from the daily average archive of the simulation:

21699291, 2022, 3, Downloaded from https://agupubs.onlinelibrary.wiley.com/doi/10.1029/2020JC017114 by Cochrane France, Wiley Online Library on [16/03/2023]. See the Terms and Conditions (https://onlinelibrary.wiley.com/terms-and-conditions) on Wiley Online Library for rules of use; OA articles are governed by the applicable Creative Commons License

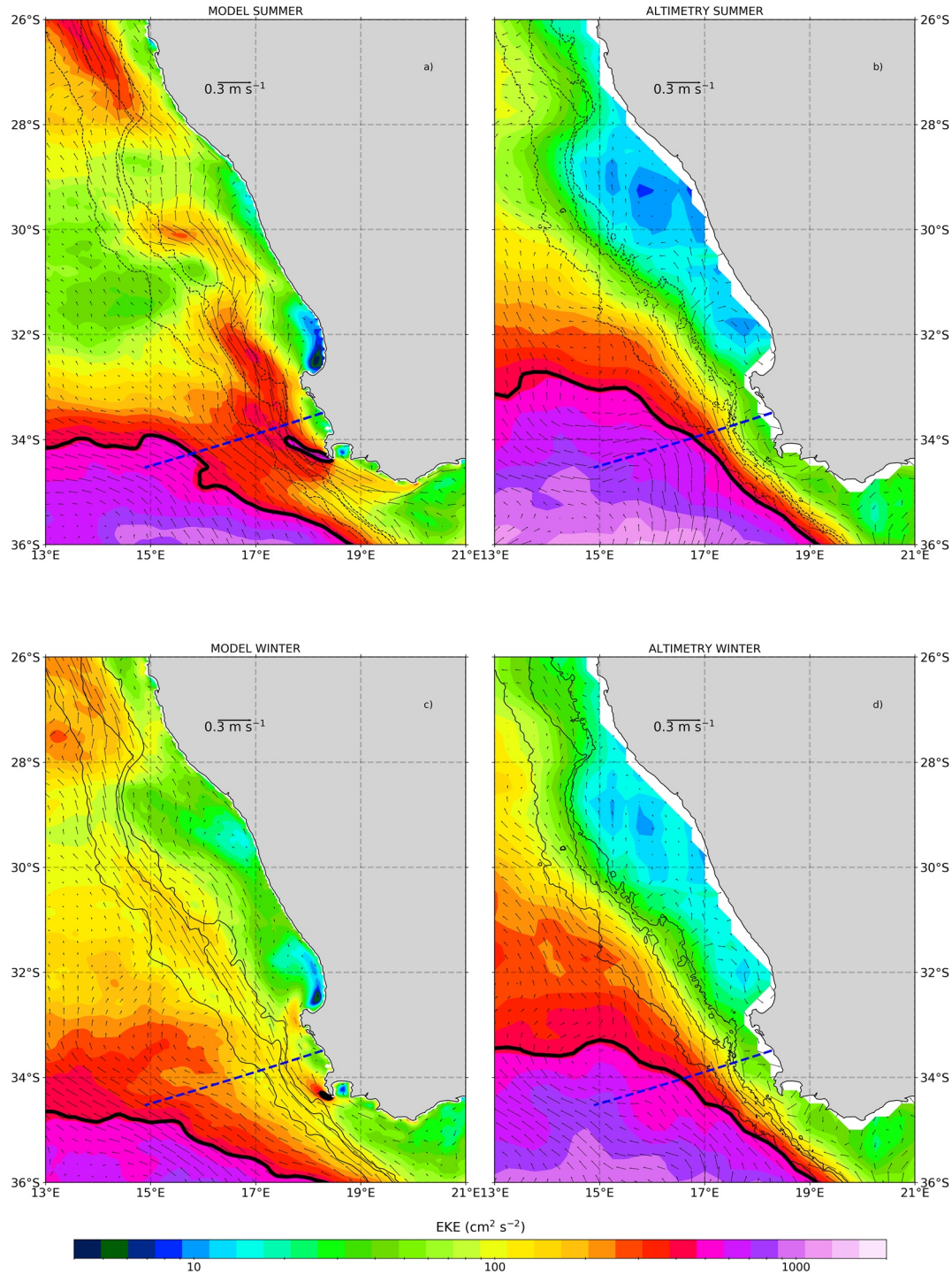

Figure 3. Summer (top) and winter (bottom) climatology of surface geostrophic Eddy Kinetic Energy (EKE) with corresponding surface geostrophic currents superimposed for the R3KM simulation (left) and satellite altimetry data (right). The 450 $cm^2\ s^{-2}$ contour, delimiting the extension of the high EKE values typically found in the region affected by the Agulhas Current retroflection (Loveday et al., 2014) is superimposed (thick black), as well as the 200 and 500 m and 2,000 m isobaths (solid black), and the transect off Grotto Bay (thick blue).

21699291, 2022, 3, Downloaded from https://agupubs.onlinelibrary.wiley.com/doi/10.1029/2020JC017114 by Cochrane France, Wiley Online Library on [16/03/2023]. See the Terms and Conditions (https://onlinelibrary.wiley.com/terms-and-conditions) on Wiley Online Library for rules of use; OA articles are governed by the applicable Creative Commons License

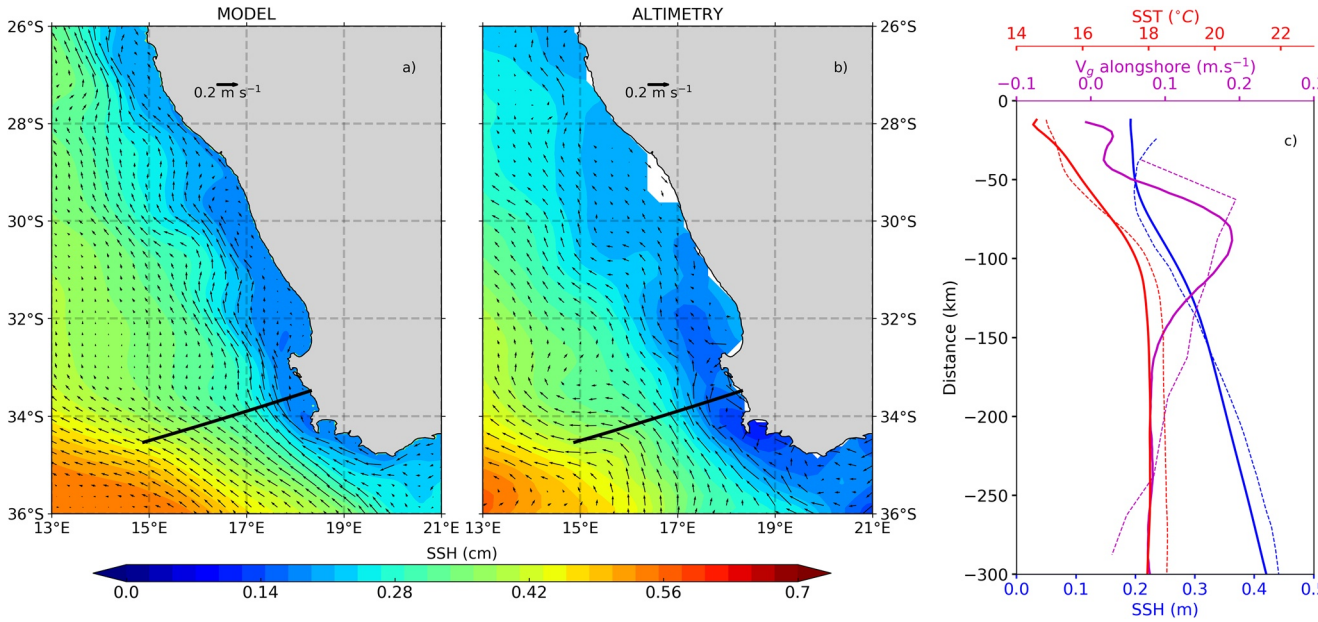

Figure 4. Annual average of sea surface height (SSH) with corresponding surface geostrophic currents superimposed: (a) model outputs averaged over 1992–2011; (b) satellite absolute dynamic topography (ADT) data averaged over 1993–2010; (c) across-shore profiles of model (solid) and satellite (dashed) annual averages of SST (red), ADT (blue), and along-shore geostrophic current (magenta) off Grotto Bay (black line in a) and (b). The plotted model SSH was offset by +0.52 m so that the model and satellite spatially average fields matched over the domain of interest. The origin of the distance axis is at the coast.

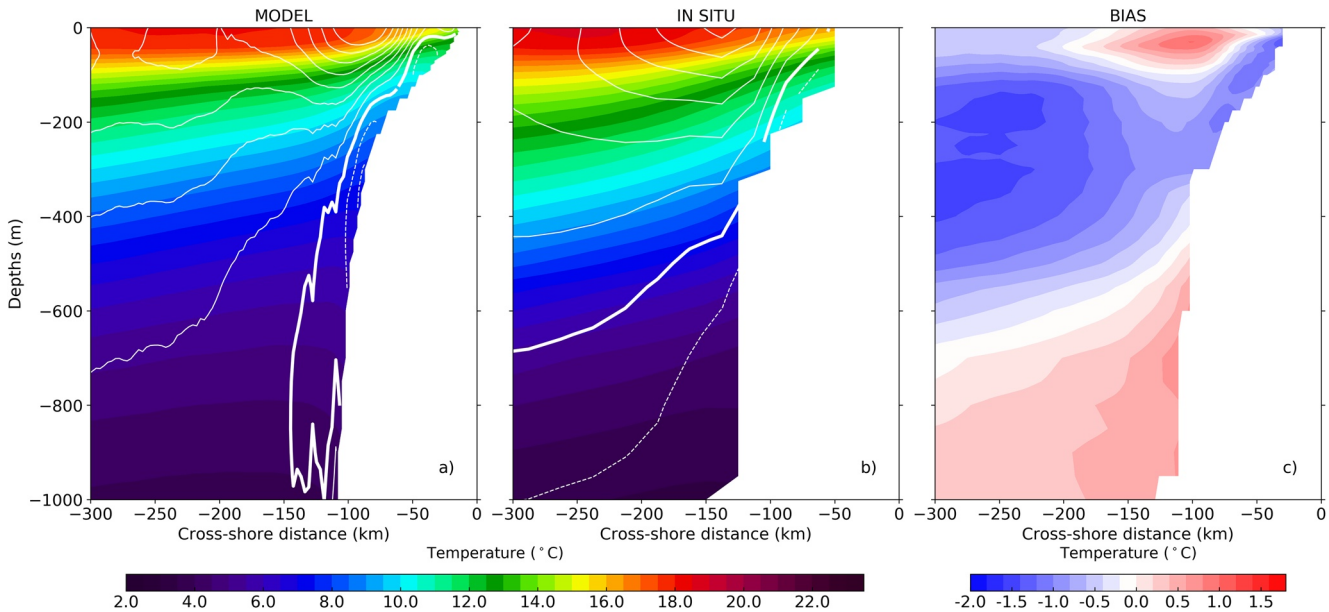

Figure 5. Temperature transect off Grotto Bay (solid black line on Figure 4) with the along-shore component of the geostrophic current superimposed (white contours). (a) World Ocean Atlas annual average (WOA18; Garcia et al., 2018); (b) Same as in (a) for the model; (c) Temperature bias ($T_{model} - T_{WOA2018}$). Geostrophic velocities are built with a reference level at 1,000-m depth for the WOA18 data and at surface for the model. The intensity of the geostrophic velocity at the reference level is equal to the surface geostrophic velocity derived from sea surface height for the model and null for WOA18 data. Contours are plotted every 0.02 m s^{-1} in the range [−0.04 0.16] m s^{-1}. Negative values are dashed.

21699291, 2022, 3, Downloaded from https://agupubs.onlinelibrary.wiley.com/doi/10.1029/2020JC017114 by Cochrane France, Wiley Online Library on [16/03/2023]. See the Terms and Conditions (https://onlinelibrary.wiley.com/terms-and-conditions) on Wiley Online Library for rules of use; OA articles are governed by the applicable Creative Commons License

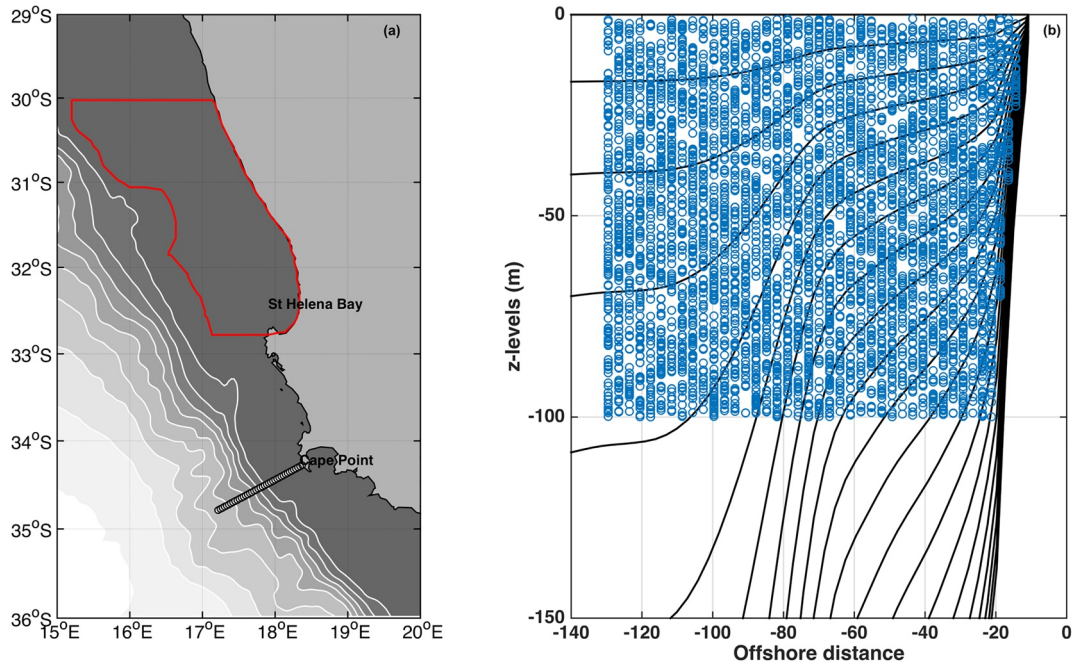

Figure 6. (a) R3KM model bathymetry (gray with a contour interval of 500 m). Particles are released between the surface and −100 m along the SARP line, an across-shore transect off Cape Point (white circles). The target region, delineated by the red polygon, corresponds to St Helena Bay. A particle is considered successful if it reaches the target area within 30 days. (b) One random sample of the initial vertical distribution of particles off Cape Point during a release event (blue circles). Terrain following sigma levels of the R3KM model are superimposed in black.

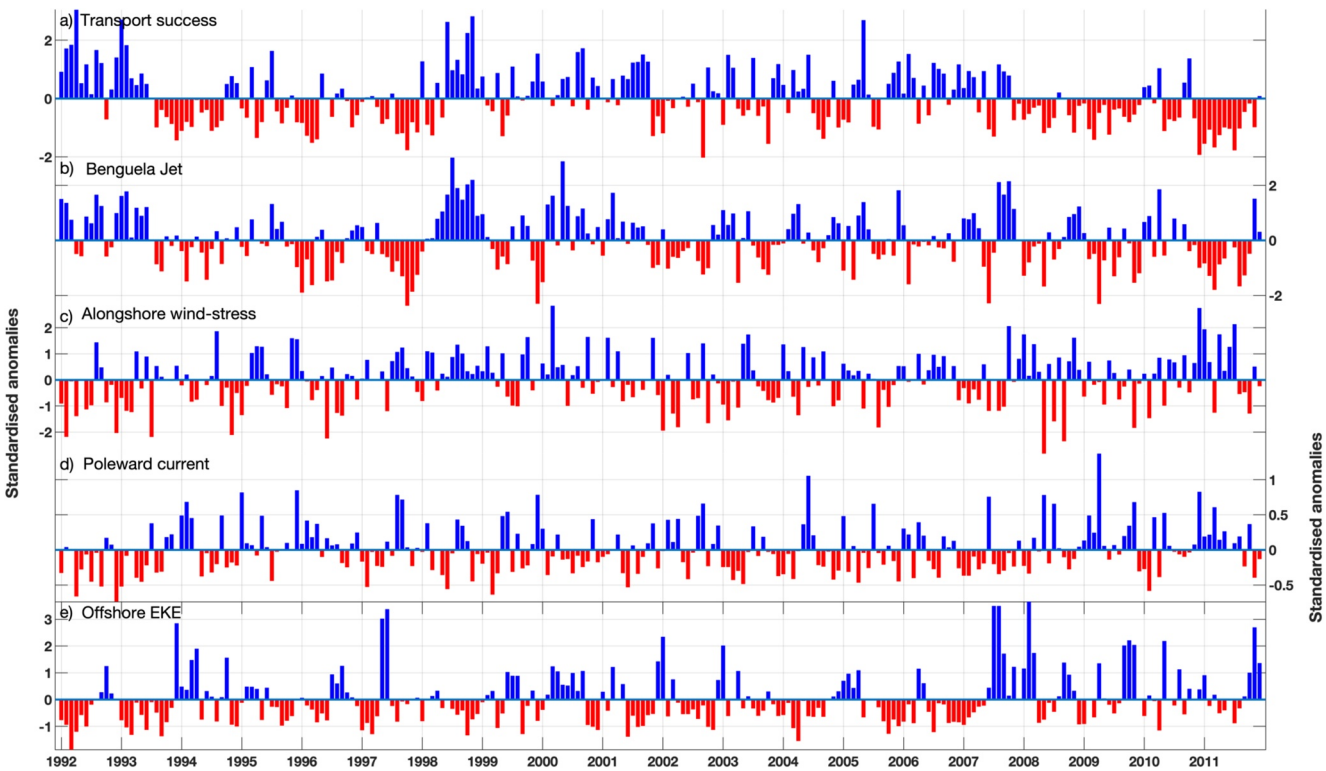

Figure 7. Time series, over the 1992–2011 period, of the normalized monthly anomalies of: (a) transport success (TS′); (b) Benguela jet Intensity; (c) Poleward inshore counter-current; (d) offshore EKE.

21699291, 2022, 3, Downloaded from https://agupubs.onlinelibrary.wiley.com/doi/10.1029/2020JC017114 by Cochrane France, Wiley Online Library on [16/03/2023]. See the Terms and Conditions (https://onlinelibrary.wiley.com/terms-and-conditions) on Wiley Online Library for rules of use; OA articles are governed by the applicable Creative Commons License

$$I_{is}(iy) = \frac{1}{n(iy, is)} \Sigma_{is} I\left(id(iy, is)\right), \tag{1}$$

where I_{is} is the seasonal average value of indicator I, $is = [1, \cdots 4]$ the season index (summer, autumn, winter, spring), $iy = [1992, \cdots 2011]$ the year index, and $n(iy, is)$ the number of days for season is of year iy.

2. The seasonal standardized anomalies are then computed by subtracting the seasonal climatology $\overline{I}_{is}$ and then dividing by the annual standard deviation computed over the whole 20 years σ_I

$$\begin{aligned} I'_{is}(iy) &= \frac{I_{is}(iy) - \overline{I}_{is}}{\sigma_I}, \\ \overline{I}_{is}(iy) &= \frac{1}{n_y} \Sigma_{iy} I(iy, is), \quad \text{with } n_y = 20, \text{the number of years} \\ \sigma_I &= \frac{1}{6940} \Sigma_{id=1}^{id=6940} \left(I(id) - \overline{I} \right)^2, \\ \overline{I} &= \frac{1}{6940} \Sigma_{id=1}^{id=6940} I(id). \end{aligned} \tag{2}$$

3. Correlations are computed for each season separately. Over the 20-year period of interest, for each season, we used an interannual time series of 20 seasonally average values. The number of degrees of freedom used to calculate the p-value was therefore $20-1 = 19$. The four seasons are built to match with the early upwelling season in spring (September–November), the peak upwelling season in summer (December–February), the late upwelling season in autumn (March–May), and the non-upwelling season in winter (June–August). The seasonal averaging allows to smooth out the time series and to better account for each season specificity (upwelling vs. non-upwelling) by integrating the physical processes inherent to each season over a 3-month period.

The monthly time series are built exactly the same way. One may replace the season index is by a monthly index $im = [1, \cdots 12]$ in above steps 1 and 2.

3.2. The 1992–2011 Time Series of Monthly Transport Success Anomalies

The time series of normalized monthly transport success anomalies computed from our set of Lagrangian experiments reveals a strong inter-annual variability (Figure 7). Although the signal appears to be highly variable on a monthly time scale, notable longer periods of positive and negative transport success can be spotted. The time series starts with a short period of positive anomalies from 1992 to mid-1993. This period is followed by a 4-year period of negative transport success anomalies from 1993 to 1997. In 1997, transport success anomalies shift back toward positive values for the subsequent 3 years from 1998 to 2001. The years 2002–2005 appear to be more variable, with positive and negative monthly transport success anomalies randomly distributed. Nevertheless, after 2006, the time series starts fluctuating again with a more stable pattern and a roughly 3-year period. The years 2006–2008 are marked by positive transport success anomalies whereas the years 2008–2011 are characterized by negative anomalies.

3.3. Correlations With Indicators of the Key Features of the Local Dynamics

3.3.1. Influence of the Benguela Jet

The intensity of the Benguela Jet (Veitch et al., 2017) is computed as the depth-integrated (top 100 m) alongshore current velocity anomalies averaged over the 200–500 m isobaths from Cape Point (34°S) to north of Cape Columbine (32°S; Figure 8a). Scatter plots of this indicator versus transport success show that positive correlation is significant all year round, and peaks in summer (Figure 8b). These positive correlations indicate that positive (negative) transport success anomalies can be attributed to a stronger (weaker) Benguela Jet intensity.

21699291, 2022, 3, Downloaded from https://agupubs.onlinelibrary.wiley.com/doi/10.1029/2020JC017114 by Cochrane France, Wiley Online Library on [16/03/2023]. See the Terms and Conditions (https://onlinelibrary.wiley.com/terms-and-conditions) on Wiley Online Library for rules of use; OA articles are governed by the applicable Creative Commons License

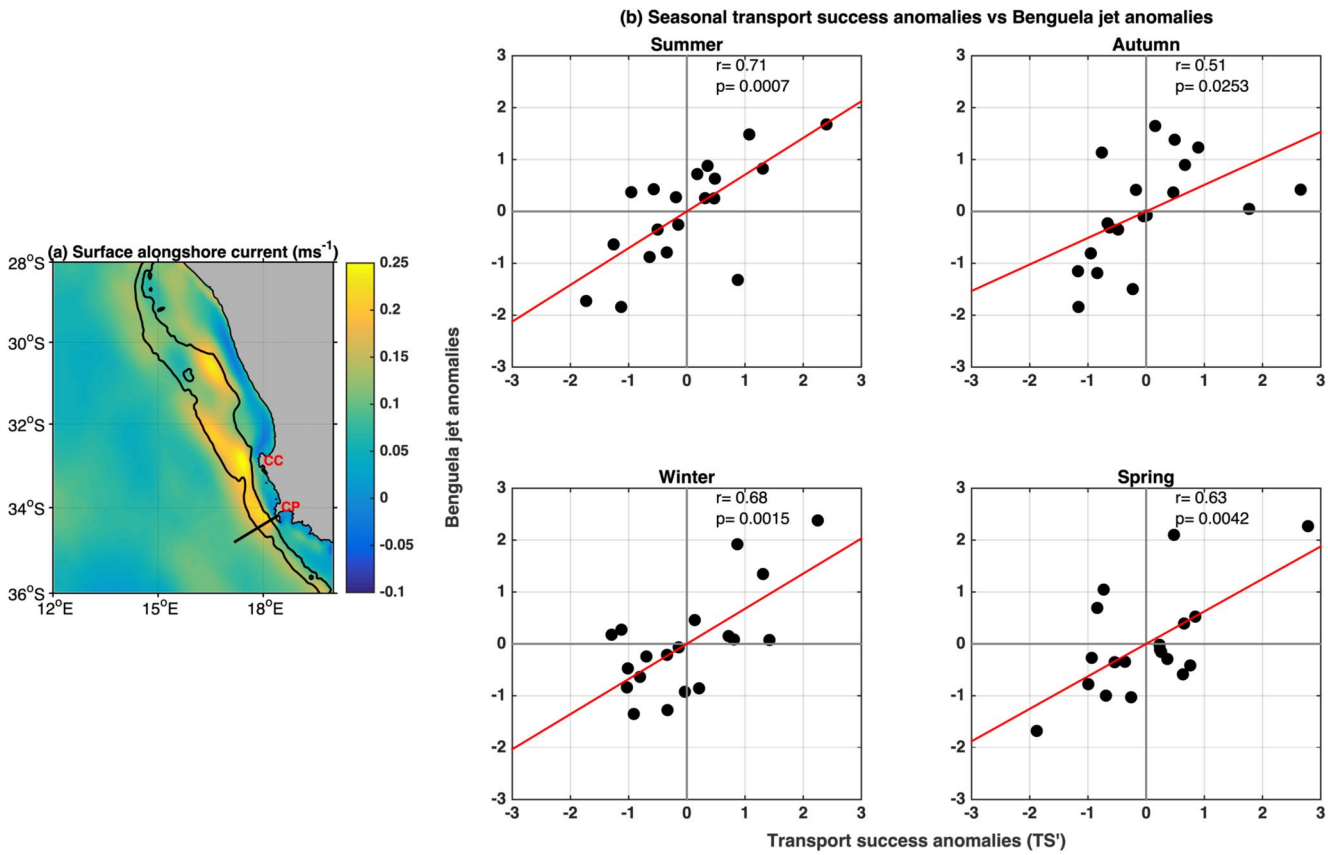

Figure 8. (a) R3KM simulation annual climatology of surface alongshore current velocities (m s^{-1}). The 200 and 500 m isobaths are superimposed in black. (b) Seasonal scatter plots of transport success anomalies against anomalies of the strength of the Benguela Jet. All anomalies are seasonal normalized anomalies. The strength of the Benguela Jet is computed by averaging the depth-integrated (top 100 m) along-shore velocity between Cape Point (34°S) and St Helena Bay (32°S) over the 200–500 m isobaths. A positive (negative) anomaly suggests a stronger (weaker) northward jet.

3.3.2. Influence of the Along-Shore Winds

Upwelling-favorable equatorward alongshore winds (Figure 9a) drive an offshore Ekman transport that favors the cross-shelf transport of surface particles, and therefore contributes to remove inshore particles from the Benguela Jet. A significant negative relationship ($r = -0.6$, $p < 0.05$) is found between anomalies of transport success and alongshore equatorward wind stress during the summer upwelling season. This negative correlation highlights the offshore loss of particles by offshore Ekman transport during the occurrence of strong equatorward wind stress (positive anomalies).

3.3.3. Influence of the Inner-Shelf Poleward Counter-Current

The R3KM simulation shows bursts of an inner-shelf poleward counter-current during the upwelling season consistent with the observations of Brown and Hutchings (1987) and Fawcett et al. (2008). These events of poleward flow are also associated with southward particles' trajectories, in the opposite direction of St Helena Bay. Events showing the presence of this poleward counter-current are therefore spotted by averaging, on the SARP line, the southward velocities only ($v < 0$) within the top 100 m of the water column and over the inner-shelf region delineated by the 50-km coastal band (Figure 10a). The absolute values of the velocities are used to calculate anomalies of the inner-shelf counter-current, with positive (negative) anomalies corresponding to a stronger (weaker) than average poleward flow. Our analysis shows that there is a significant negative correlation between TS and the presence of such poleward counter-current in summer ($r = -0.68$, $p < 0.05$), autumn ($r = -0.56$, $p < 0.05$), winter ($r = -0.49$, $p < 0.05$) but none in spring (Figure 10b).

21699291, 2022, 3, Downloaded from https://agupubs.onlinelibrary.wiley.com/doi/10.1029/2020JC017114 by Cochrane France, Wiley Online Library on [16/03/2023]. See the Terms and Conditions (https://onlinelibrary.wiley.com/terms-and-conditions) on Wiley Online Library for rules of use; OA articles are governed by the applicable Creative Commons License

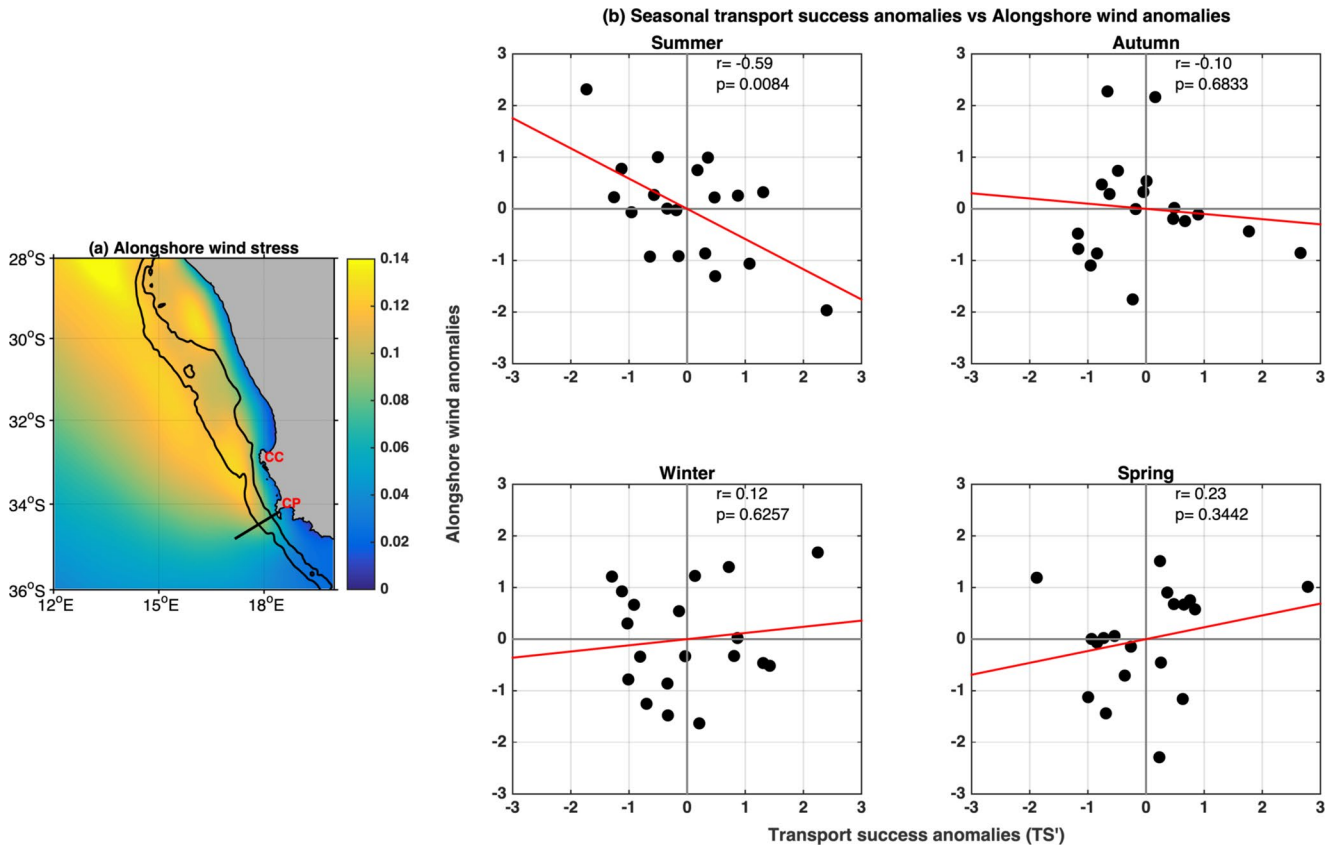

Figure 9. (a) R3KM climatology of alongshore wind stress (m s^{-1}) for January. The 200 and 500 m isobaths are superimposed in black. (b) Seasonal scatter plots of transport success anomalies against anomalies of the alongshore wind stress. The latter is averaged over the across-shore Cape Point transect (thick black line in (a)). A positive (negative) alongshore wind anomaly suggests stronger (weaker) equatorward winds.

3.3.4. Influence of the Off-Shelf Mesoscale Turbulence

Ragoasha et al. (2019) showed that particles initially released off-shore, beyond the 500-m isobath, had a very low probability of reaching St Helena Bay. They related this low probability to the presence of an intense mesoscale eddy activity just off the shelf edge (Veitch et al., 2009; Veitch & Penven, 2017). The following analysis intends to analyze the effective role of the off-shelf turbulence in driving the inter-annual variability of transport success. Seasonal EKE anomalies, a proxy for mesoscale turbulence, are spatially averaged over the outer shelf-slope (500–3,000 m) between Cape Point and Cape Columbine, and plotted against seasonal transport success anomalies (Figure 11b). A significant negative correlation ($r = -0.54$, $p < 0.05$) is found during the summer season only. Ragoasha et al. (2019) hypothesized that peaks in offshore Ekman transport during summer would result in most shelf particles being advected offshore, within an area dominated by high mesoscale activity (Figure 11a), which in turn would induce more chaotic particles' trajectories, and therefore reduce their chance of reaching St Helena Bay.

3.4. Disentangling the Role of Each Individual Process

The above analysis has shown that there are multiple physical processes that impact the inter-annual variability of transport success. However, some of the extended periods of negative and positive anomalies in Figure 7 could be traced back to some common patterns and combination of the physical drivers. The positive events over the periods 1992–1993 and 1998–2001 coincided with an anomalously stronger Benguela Jet, some reduced intensity of the upwelling favorable winds (except for 1998), and some weakness or absence of the inner-shelf poleward counter-current. In 1998, the unusual strength of the Benguela Jet seems to have inhibited the expected offshore loss of particles due to increased offshore Ekman transport. The negative periods of 1994–1997 and 2011 coincided with the exact opposite combination, that is, a weaker than average Benguela Jet, more sustained

21699291, 2022, 3, Downloaded from https://agupubs.onlinelibrary.wiley.com/doi/10.1029/2020JC017114 by Cochrane France, Wiley Online Library on [16/03/2023]. See the Terms and Conditions (https://onlinelibrary.wiley.com/terms-and-conditions) on Wiley Online Library for rules of use; OA articles are governed by the applicable Creative Commons License

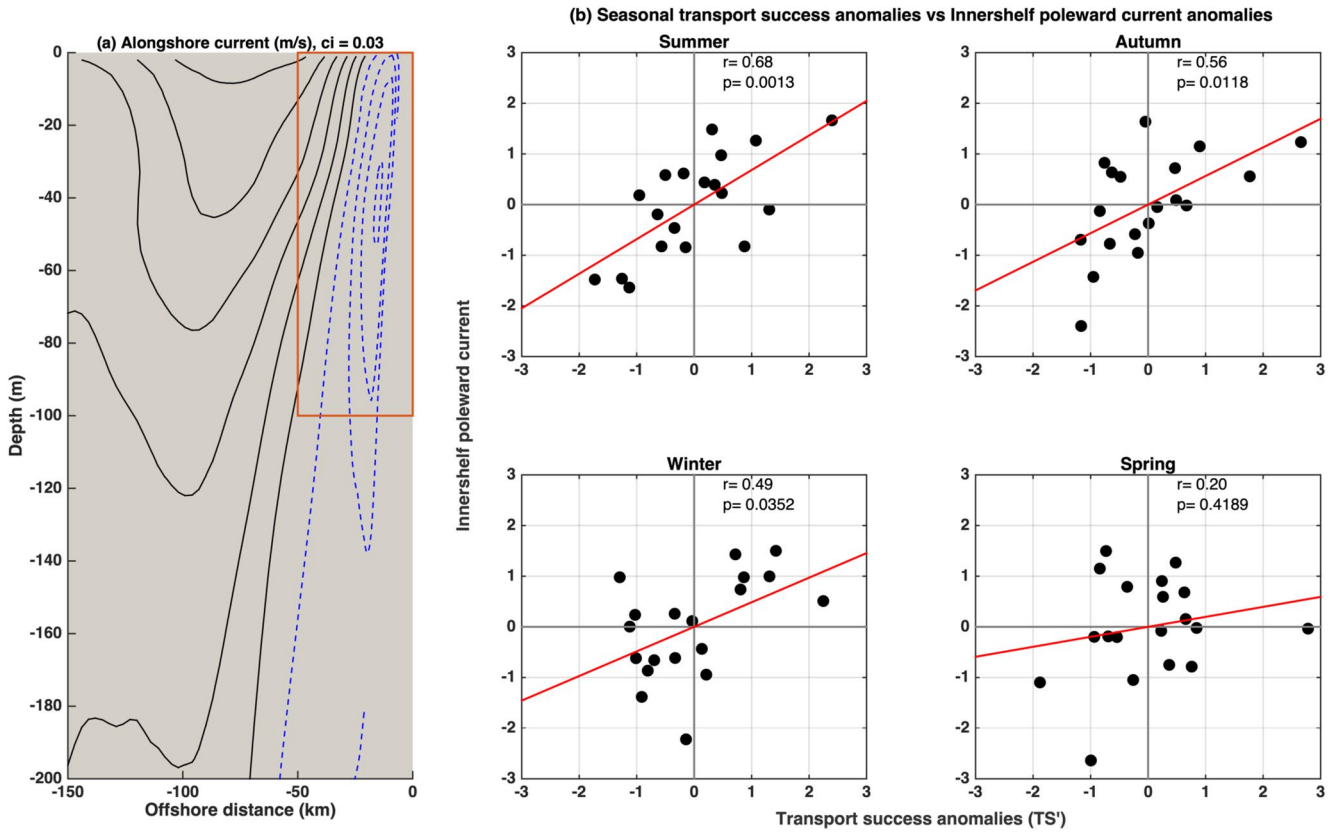

Figure 10. (a) R3KM autumn climatology of alongshore velocity contours across the Cape Point transect (black line in (a)). The contour interval is 0.03 m s^{-1}. Positive/negative velocities are shown in solid-black/blue-dashed lines. (b) Seasonal scatter plots of transport success anomalies against anomalies of the inner-shelf poleward counter-current. The poleward current anomalies are derived by averaging only negative velocities ($v < 0$) over the 50-km coastal band and integrated over the top 100-m depth at a transect off Cape Point (orange box). A positive (negative) current anomaly suggests a stronger (weaker) poleward current.

upwelling favorable winds, and an increased signature of the inner-shelf poleward counter-current. However, for most events, no such simple pattern or combination emerge. In addition, the exact effect on transport success of off-shelf eddies seems hard to predict, and highly sensitive to the type of eddies, their strength, the exact position relative to the shelf itself, and even their interaction with each other.

4. The Inshore and Offshore Routes Contributions to Transport Success

Offshore and inshore routes had been identified as the two main Lagrangian pathways for particles successfully traveling from Cape Point to St Helena Bay (Ragoasha et al., 2019). The inshore route corresponds to particles advected by the Benguela Jet. It is a fast and efficient route for particles released on the shelf. The offshore route corresponds to particles released on the outer shelf edge. It is less efficient and slower, as particles' trajectories are more chaotic due to the presence of mesoscale eddies in the off-shelf area. The following section intends to investigate whether the inter-annual variability in the time series of transport success (Figure 7) could be explained by some variability in the contribution and efficiency of these two routes, and the sudden disappearance or growth of one of the two identified pathways.

4.1. Quantifying Both Contributions and the Interconnections Between the Two Routes

Taking a similar approach to Ragoasha et al. (2019), particles are therefore subsequently divided into a group of particles released inshore of the 500-m isobath and another group of particles released further off-shore. The monthly transport success becomes the sum of two contributions: $TS_m = TSI_m + TSO_m$, with TSI_m and TSO_m the monthly transport success of the inshore and offshore group, respectively. These two new variables are standardized as follows:

21699291, 2022, 3, Downloaded from https://agupubs.onlinelibrary.wiley.com/doi/10.1029/2020JC017114 by Cochrane France, Wiley Online Library on [16/03/2023]. See the Terms and Conditions (https://onlinelibrary.wiley.com/terms-and-conditions) on Wiley Online Library for rules of use; OA articles are governed by the applicable Creative Commons License

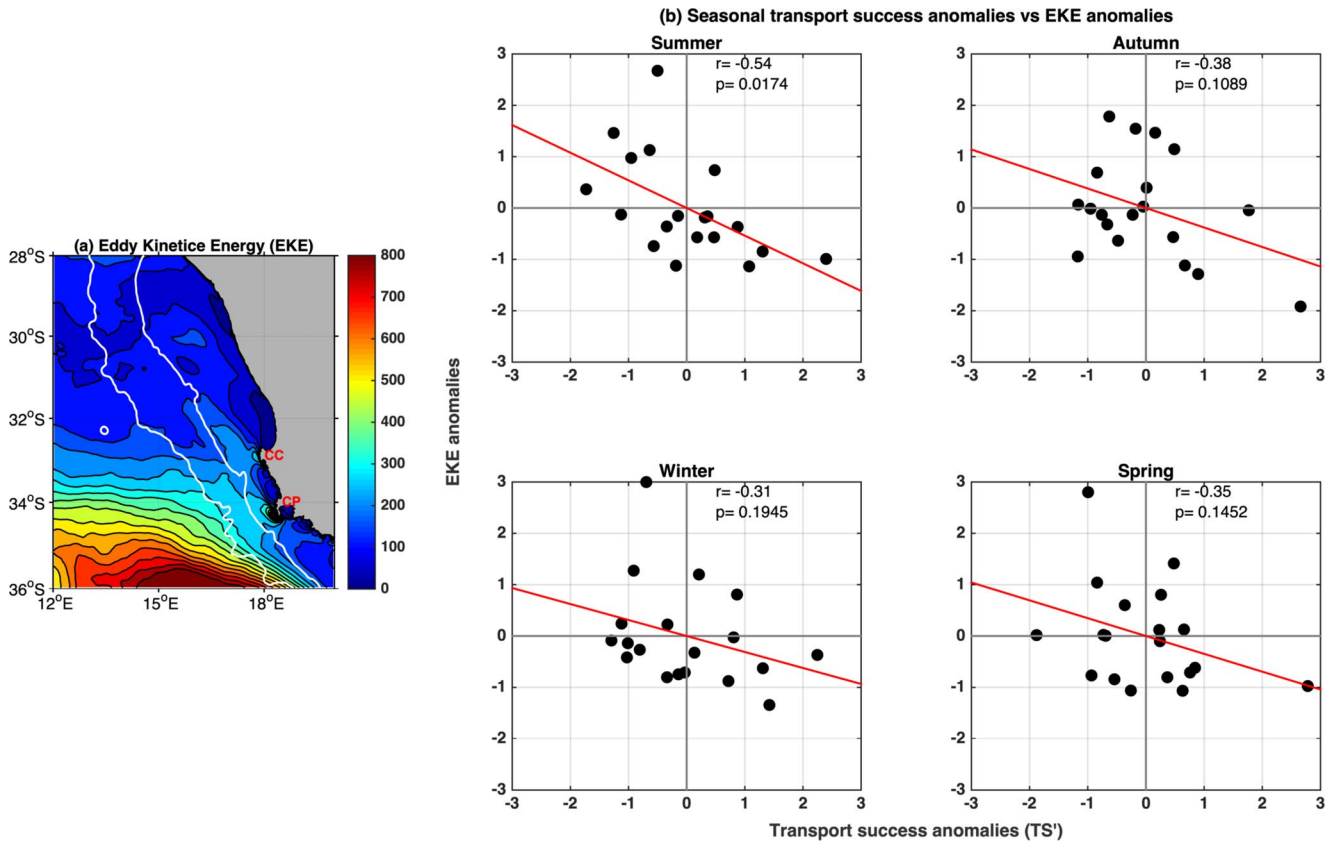

Figure 11. (a) Annual climatology of surface EKE ($cm^{-2}s^{-2}$). The 500 and 3,000 m isobaths are superimposed in white. (b) Same as in Figures 8b, 9b, and Figure 10b but for normalized transport success anomalies against EKE anomalies. The EKE anomalies are averaged over the area between Cape Point (34°S) and Cape Columbine (33°S) bounded by the shelf edge (500-m isobath) and the 3,000-m isobath. A positive (negative) EKE anomaly suggests a stronger (weaker) mesoscale turbulence.

$$TSI'_m = \frac{TSI_m - \overline{TSI_m}}{\sigma_{TS}},$$
$$TSO'_m = \frac{TSO_m - \overline{TSO_m}}{\sigma_{TS}}, \quad (3)$$

where the $\bar{\cdot}_m$ represents a monthly climatology operator. The standardized anomalies have been normalized by the annual standard deviation of the total transport success σ_{TS}, which allows us to plot their time series in a cumulative bar graph: $TS'_m = TSI'_m + TSO'_m$ (Figure 13).

Once the contribution of the inshore and offshore particles has been obtained, interconnections between the two groups are investigated. Across-shelf advection processes may be capable of sweeping particles from one route to the other and vice-versa. To infer the existence of cross-roads between the two routes, the inshore and offshore groups of particles are further subdivided into four subgroups according to the individual across-shore cumulative displacement of the particles. We then compute the relative contribution of each subgroup to the transport success.Characteristics of the four subgroups are resumed in Table 1 and examples of particles' trajectory for the four subgroups are presented in Figure 12. When, on its journey to St Helena Bay, a particle is spotted over an isobath which is 50 km more offshore than its initial isobath, it is considered as having experienced a significant across-shelf displacement, and it is assigned to a more offshore subgroup. This analysis allows us to consider the contribution of successful inshore particles that actually remained inshore versus those that experienced an off-shore journey and were then advected back inshore. This subdivision also allows us to infer whether some particles, that were initially located on the outer-shelf, still managed to come back inshore and enter the target area, despite having experience very offshore trajectories. Details on the computations of the across-shore displacement are given in Appendix A.

21699291, 2022, 3, Downloaded from https://agupubs.onlinelibrary.wiley.com/doi/10.1029/2020JC017114 by Cochrane France, Wiley Online Library on [16/03/2023]. See the Terms and Conditions (https://onlinelibrary.wiley.com/terms-and-conditions) on Wiley Online Library for rules of use; OA articles are governed by the applicable Creative Commons License

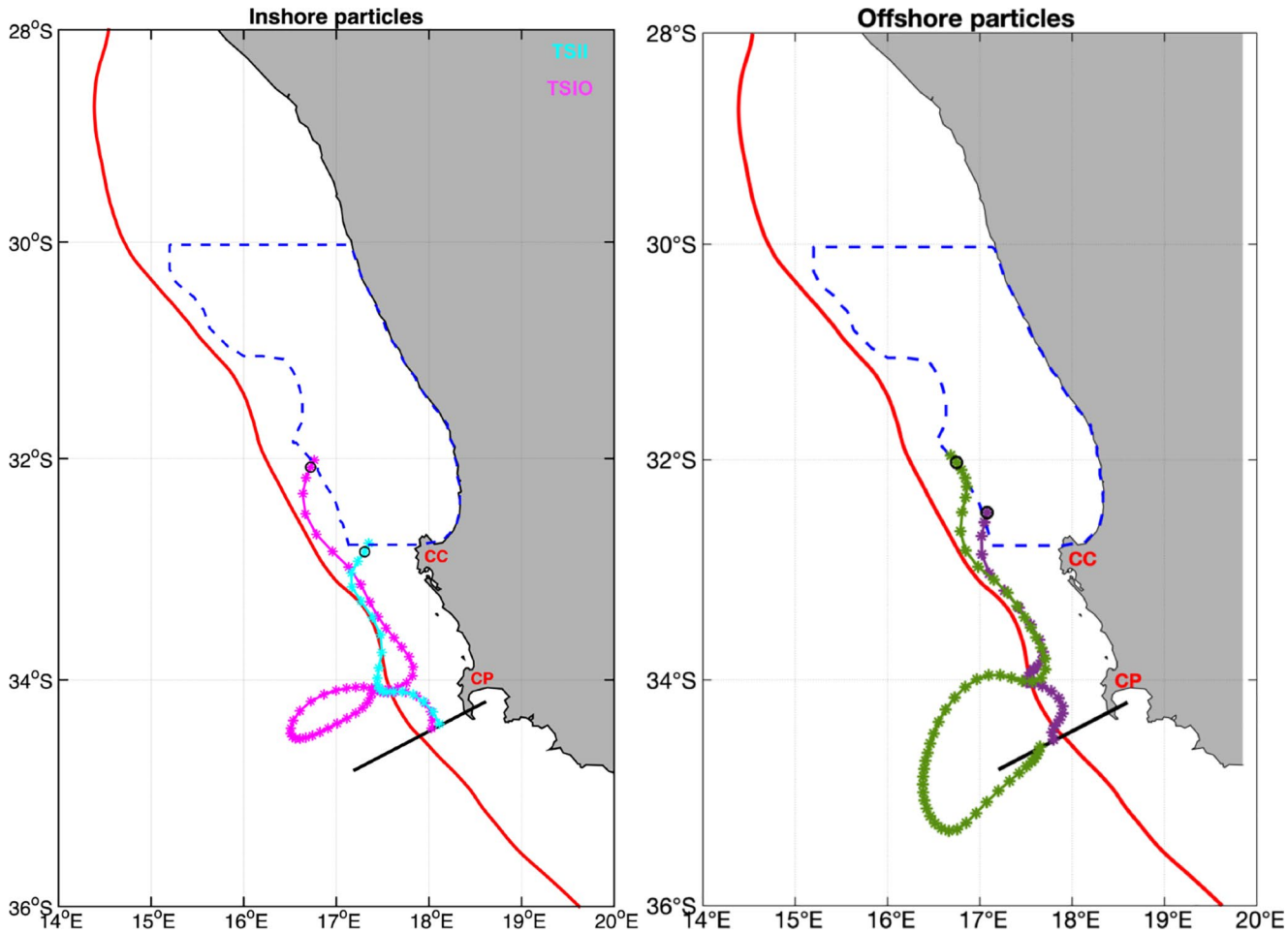

Figure 12. Four typical trajectories of successful particles. (a) Particles released inshore of the 500 m isobath and advected toward St Helena Bay: one remains inshore of this isobath (cyan) and therefore belongs to the TSII subgroup, while the other experiences and offshore loop (magenta) and therefore belongs to the TSIO subgroup. (b) Particles released beyond the 500 m isobath and advected toward St Helena Bay: one remains close to its initial isobath (purple) and therefore belongs to the TSOI subgroup, while the other experiences an offshore excursion (green) and therefore belongs to the TSOO subgroup.

4.2. The Relative Contribution of Inshore and Offshore Particles

The cumulative monthly time series (Figure 13) confirms that both the inshore and offshore groups of particles contribute to the observed variability of TS'_m. In addition, the TSI′ and TSO′ time series are both strongly correlated with TS′ ($r = 0.83$ and $r = 0.84$, respectively, and $p < 0.05$). Nevertheless, the relative contribution of each group varies according to the signs of TS'_m. For $TS'_m < 0$, the negative anomalies associated with inshore particles (blue bars on Figure 13) have a more significant role to play than the ones associated with the offshore particles (orange bars): |TSI| > |TSO| and a higher correlation coefficient is found between TS′ and TSI′ ($r = 0.71$) than in between TS′ and TSO′ ($r = 0.53$). In contrast, for the largest values of $TS'_m > 0$, the relative contribution of offshore particles (orange bars) dominates: |TSO| > |TSI|.

In an attempt to identify the physical processes impacting the TSI′ and TSO′ time series, the seasonal inshore and offshore transport success anomalies were correlated with the same indicators of the local dynamics used in Section 3. Results are presented in Table 2, and are consistent with our previous findings. No significant correlation was found between anomalies of the Benguela Jet, the poleward current, alongshore wind stress, and offshore transport success; therefore, they are not shown in Table 2. The specific role played by the Benguela Jet in conveying the inshore particles is confirmed. Stronger than average upwelling favorable winds are unfavorable for TSI ($r = -0.68$) as well as bursts of the poleward inner-shelf counter current. Not surprisingly, offshore particles are shown to be particularly sensitive to the variability of the offshore EKE, in particular in summer and autumn, when the offshore turbulence intensifies near the shelf edge (Figure 3), which leads to negative correlations

21699291, 2022, 3, Downloaded from https://agupubs.onlinelibrary.wiley.com/doi/10.1029/2020JC017114 by Cochrane France, Wiley Online Library on [16/03/2023]. See the Terms and Conditions (https://onlinelibrary.wiley.com/terms-and-conditions) on Wiley Online Library for rules of use; OA articles are governed by the applicable Creative Commons License

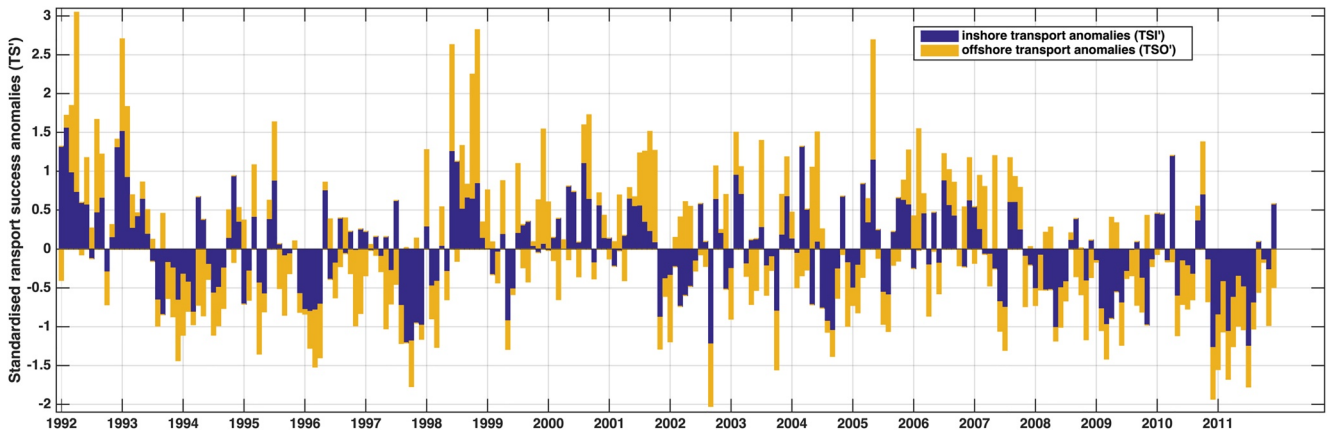

Figure 13. Same as Figure 7a, but the monthly transport success anomalies are now plotted as cumulative bars showing the contribution of the inshore (TSI′: blue) and offshore (TSO′: orange) particles.

between the seasonally averaged EKE anomalies and TSO′ ($r = -0.52$ in summer and $r = -0.56$ in autumn, with $p < 0.05$). Inshore particles are also negatively affected by the presence of large EKE values in the offshore region in summer only ($r = -0.47$ $p < 0.05$), when the surface Ekman drift induced by upwelling favorable winds pushes the inshore particles offshore toward the intense mesoscale eddy field.

4.3. The Across-Shelf Displacements of Inshore and Offshore Particles

Standardized transport success anomalies are calculated for the four subgroups of particles (Table 1) in a similar way to TSI′ and TSO′ (Equation 3). Time series are plotted in Figure 14. The TSI′ and TSII′ time series are highly coherent ($r = 0.85$, $p < 0.05$), and their variability directly links to the number of particles capable of remaining inshore of the 500-m isobath, that is, embedded within the Benguela Jet. The largest negative TSII′ < 0 are the main contributors to the largest negative TSI′, and therefore TS′ also, suggesting that the offshore removal of inshore particles is the most important physical driver of the weak transport success events.

The contribution to transport success of the inshore particles looping offshore before coming back inshore to enter St Helena Bay (TSIO subgroup) appears to be weak over most of the time series, except between 2002 and 2005 where negative and positive values seem randomly distributed. In addition, no significant correlation was

Table 1
Characteristics of the Four Subgroups of Successful Particles. The Subdivision is Based on the Initial Isobath and Cumulative Across-Shelf Displacement of Each Individual Particle. The First Index Refers to Whether Particles Were Released Inshore (I) or Offshore (O) of the 500-m Isobath. The Second Index Refers to Whether the Particles Experienced Inshore (I) or Offshore (O) Advection

Groups	Description
TSII	Successful particles released inshore of the 500-m isobath and never displaced more than 50-km offshore from their initial isobath.
TSIO	Successful particles released inshore of the 500-m isobath and spotted (at least once) more than 50-km offshore from their initial isobath, during their journey to St Helena Bay.
TSOI	Successful particles released offshore of the 500-m isobath, and never displaced more than 50 km from their initial isobath.
TSOO	Successful particles released offshore of the 500-m isobath and spotted (at least once) more than 50-km offshore from their initial isobath, during their journey to St Helena Bay.

21699291, 2022, 3, Downloaded from https://agupubs.onlinelibrary.wiley.com/doi/10.1029/2020JC017114 by Cochrane France, Wiley Online Library on [16/03/2023]. See the Terms and Conditions (https://onlinelibrary.wiley.com/terms-and-conditions) on Wiley Online Library for rules of use; OA articles are governed by the applicable Creative Commons License

Table 2
The Relationship Between (1) Inshore Transport Success Anomalies and the Anomalies of the Benguela Jet, Alongshore Wind, Poleward Flow, and Offshore EKE Including (2) Offshore EKE and Offshore Transport Success Anomalies. The Bold Correlation Coefficients Indicate Where the Relationship is Significant at $p < 0.05$

(1) Inshore transport success anomalies	Summer	Autumn	Winter	Spring
Benguela Jet	**0.78**	**0.66**	**0.65**	**0.68**
Alongshore wind	**−0.68**	0.21	0.20	0.05
Poleward flow	**−0.83**	**−0.65**	**−0.61**	**−0.44**
Offshore EKE	**−0.47**	0.06	−0.20	−0.21
(2) Offshore transport success anomalies				
Offshore EKE	**−0.52**	**−0.56**	−0.20	−0.21

found between TSI′ and TSIO′ ($r = 0.07$). This further suggests that inshore particles that get advected offshore within the turbulent eddy field have a reduced probability of returning inshore.

Similarly, the offshore displacement of particles already originating from the off-shelf region (TSO subgroup) is analyzed. There is a positive correlation ($r = 0.9$, $p < 0.05$) between TSO and TSOI anomalies (Figure 14c), which highlights that off-shelf particles that make it to St Helena Bay do not experience an offshore deviation. In addition, a significant negative correlation ($r = -0.52$, $p < 0.05$) exists with offshore EKE anomalies in summer, possibly confirming an offshore extension of the Benguela jet and/or low mesoscale eddy activity. TSOO anomalies also correlate significantly with TSO anomalies, but the correlation is relatively weak ($r = 0.24$, $p < 0.05$; Figure 14d). This result suggests that particles from the offshore section that become displaced further offshore may sometimes return inshore and contribute significantly to offshore transport success. However, no relationship was found between this subgroup and the mesoscale turbulent activity, highlighting the chaotic behavior of this time series due to the influence of coherent eddy features.

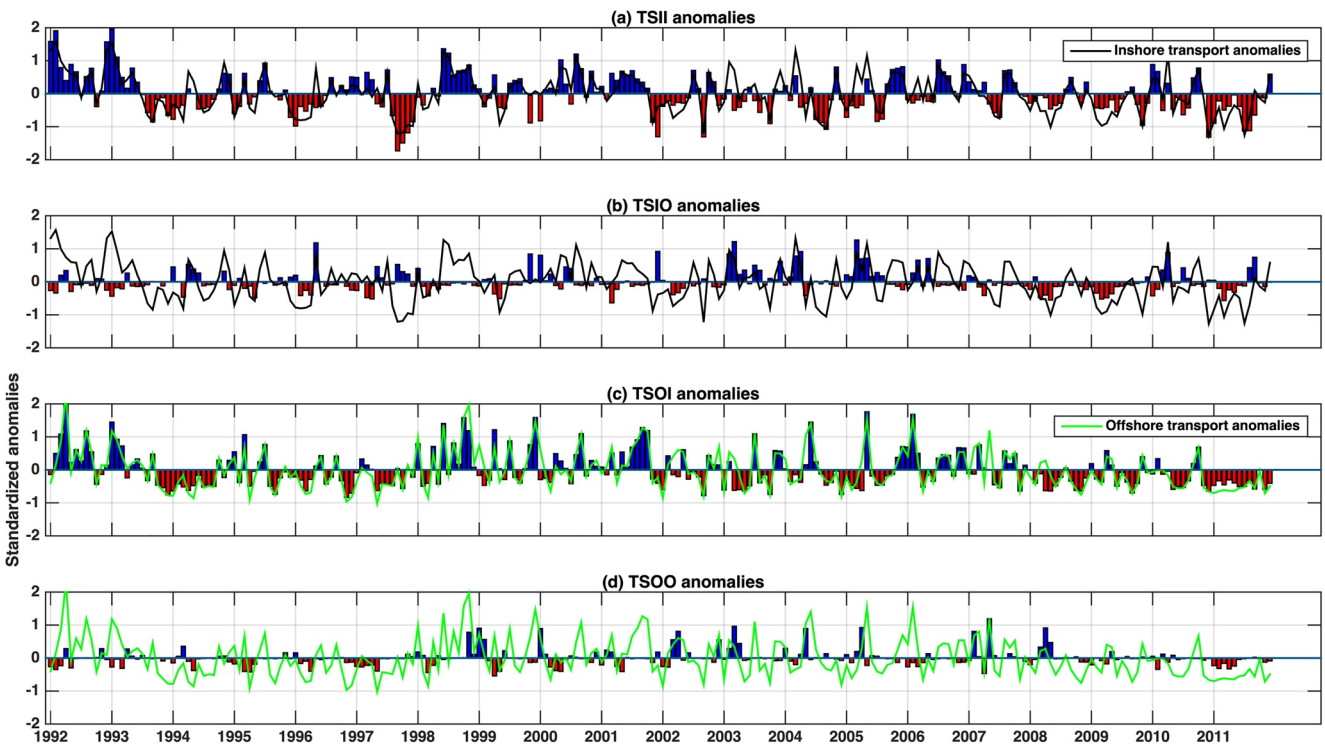

Figure 14. Standardized monthly transport success anomalies of the different subgroups of particles (Table 1). (a) and (b) $TSII'_m$ and $TSIO'_m$ (bars), respectively with the TSI'_m time series also superimposed (solid black). (c) and (d) $TSOI'_m$ and $TSOO'_m$ (bars), respectively, with the TSO'_m time series also superimposed (solid green).

21699291, 2022, 3, Downloaded from https://agupubs.onlinelibrary.wiley.com/doi/10.1029/2020JC017114 by Cochrane France, Wiley Online Library on [16/03/2023]. See the Terms and Conditions (https://onlinelibrary.wiley.com/terms-and-conditions) on Wiley Online Library for rules of use; OA articles are governed by the applicable Creative Commons License

5. The Role of Mesoscale Eddies

Our analysis has shown that some of the inter-annual variability of alongshore transport success in the southern Benguela can be explained by the combination of several factors. A retention of inshore particles over the shelf is favorable for transport success, while offshore particles need to be advected onto the shelf away from the offshore turbulence. Strong offshore Ekman transport boosts the offshore displacement of particles, whereas weak offshore Ekman transport favors inshore retention. But across-shelf transport of particles could also be attributed to temporary localized cross-shore currents induced by mesoscale eddies. Indeed, visual analysis of the particle trajectories reveals that offshore particles' trajectories are chaotic and characterized by large loops indicating their entrainment by mesoscale eddy structures. Given the sporadic nature of mesoscale eddies, their impact could be negative or positive, therefore adding spurious chaotic variability in the connectivity process. This section investigates how mesoscale eddies in the southern Benguela may have affected the inter-annual variability of transport success.

An eddy detection and tracking algorithm, similar to the one used by Halo et al. (2014) and Vianello et al. (2020) over the South-West Indian Ocean, is here applied to detect and track mesoscale eddies in the SBUS within our R3KM simulation. The values of a typical eddy displacement (X_0), eddy radius (R_0), and vorticity scale (ξ_0) were defined as 20 km, 50 km, and 10^{-5} s^{-1}, respectively. A total of 2,923 mesoscale eddies were detected and tracked during the 1992–2011 period (Figure 15), over a region encompassing 36°–32°S and 14°−20°E.

Cyclones are the vast majority (73.8%) of eddies detected in the southern Benguela. On average, they have a smaller diameter (39.9 km), a weaker amplitude (3.1 cm), and a shorter lifetime (11 days) than anticyclones (Figure 15a). About 902 of these cyclones (42%) originate from the shelf (depths <500 m; Figure 15a), and most of them remain on the shelf and propagate northwards (Figure 15c). No clear seasonal pattern was found in their generation. Anticyclones, on the other hand, are on average larger (diameter ~65.5 km), more intense (amplitude ~5.2 cm), and tend to live longer (18 days; Figure 15b). Most anticyclonic eddies originate from the very deep offshore ocean located west of South Africa. The largest ones (>150 km) correspond to Agulhas rings formed during the Agulhas Current retroflection (Figure 15b). Analyzing in detail the individual role of each detected eddy on the connectivity is beyond the scope of this study. Nevertheless, we present a set of evidences supporting some kind of general consistent behavior of some types of cyclonic and anticyclonic eddies found in the southern Benguela.

5.1. Cyclonic Eddies Influence

There is evidence that shelf-edge cyclonic eddies found between Cape Point and offshore St Helena Bay contribute to positive transport success. The eddies can lead to the onshore transport of offshore particles and reduced offshore transport of inshore particles as they mainly propagate on the shelf (Figure 15c). Figure 16 shows a positive correlation between inner-shelf EKE values, between Cape Point and the region offshore St Helena Bay, and transport success anomalies of the inshore and offshore particles. However, the correlation map shows that the correlation between EKE and TSO′ occurs slightly further north than for TSI′ (Figures 16b and 16c). Offshore transport success is in fact very sensitive to the synoptic conditions at the SARP line, which in turn, govern the early days northward along-shore advection of the particles. If offshore particles are strongly advected offshore shortly after being released, their chance of reaching St Helena Bay becomes low.

Figure 17 shows an example of how, in April 1992, the combined effect of three shelf-edge cyclonic eddies, located between Cape Point and St Helena Bay, created one of the highest positive transport success anomaly for both the inshore and offshore particles. The north-side eastward circulation of the eddies favored the onshore transport of offshore particles despite some offshore looping on the south-end. Their small size meant that less inshore particles were removed from the shelf.

5.2. Anticyclonic Eddies Influence

A negative correlation was found between transport success and offshore EKE values in the vicinity of the SARP line (Figure 16). Lagrangian trajectories give some indication that the passage of large anticyclones in this region results in strong offshore transport of particles, which could explain the negative correlation between EKE and TSO′ in this area (Figure 16c). Therefore, we focus our analysis on large anticyclones (R_{eddy} > 100 km) typical

21699291, 2022, 3, Downloaded from https://agupubs.onlinelibrary.wiley.com/doi/10.1029/2020JC017114 by Cochrane France, Wiley Online Library on [16/03/2023]. See the Terms and Conditions (https://onlinelibrary.wiley.com/terms-and-conditions) on Wiley Online Library for rules of use; OA articles are governed by the applicable Creative Commons License

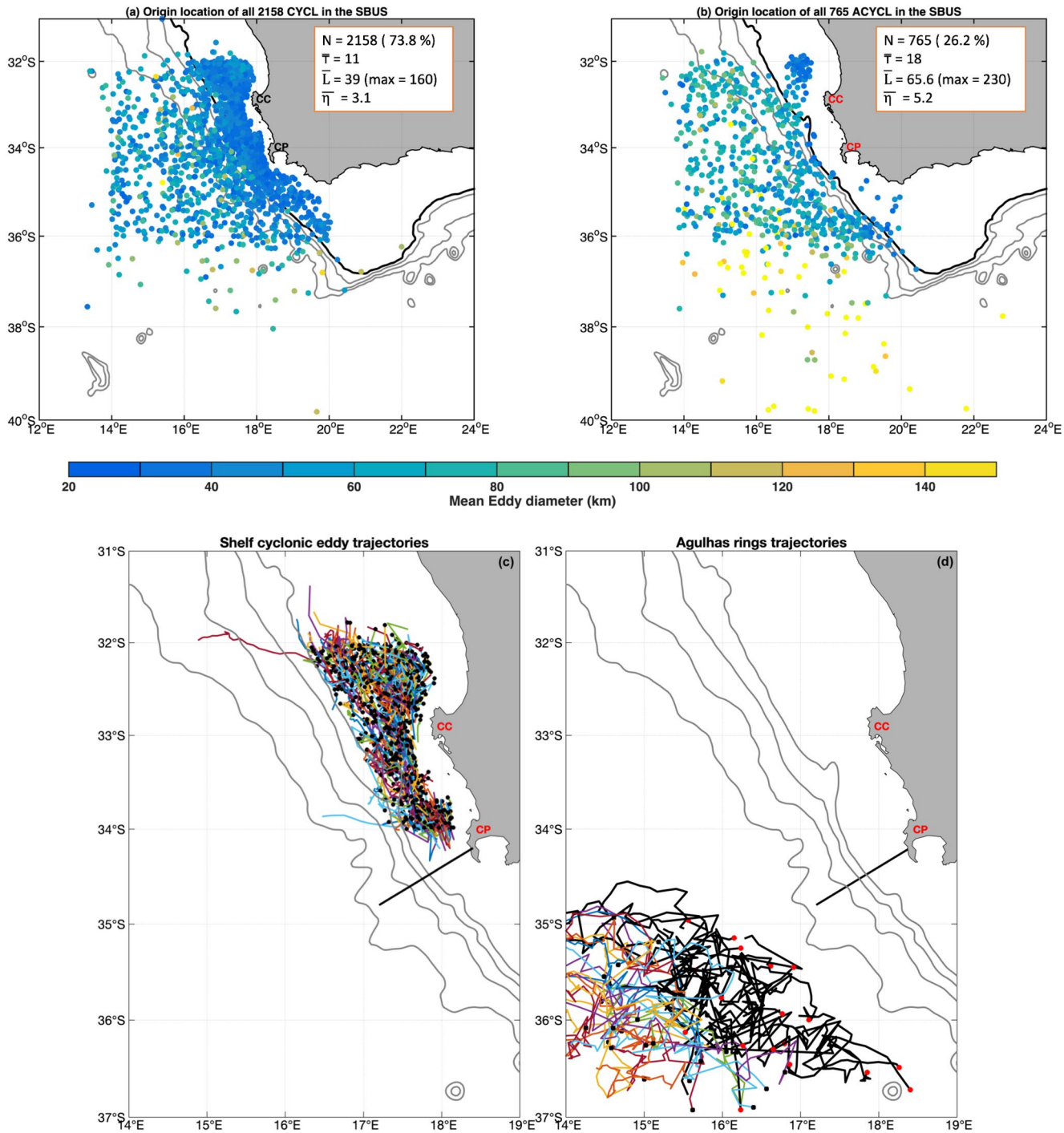

Figure 15. Generation site of all surface eddies detected over the southern Benguela (36°–32°S and 14°−20°E) within the R3KM simulation over the 1992–2011 period. Filled circles indicate the generation site of each eddy, and the color-scale its life-average diameter: (a): cyclonic eddies; (b): anticyclonic eddies. The background contours are 500 m (solid black) and 1,000 m, 2,000 m, and 3,000 m (solid gray) isobaths. The inserts show the average properties of the cyclones and anticyclones: Number of eddies (N), duration [days] $(\overline{\tau})$, diameter [km] $(\overline{L})$, diameter [km] $(\overline{\eta})$. (c) Trajectories of cyclonic eddies detected over the shelf (depth <500 m) during their lifetime. Same previous isobaths are also superimposed (solid gray) as well as the across-shore transect off Cape Point. (d) Trajectories of 18 Agulhas rings that entered into the South Atlantic following the northern route described in Dencausse et al. (2010). The ones passing nearby to the shelf are shown in black. The rest of the rings traveled toward the open ocean. Black circles indicate the generation site of each eddy.

21699291, 2022, 3, Downloaded from https://agupubs.onlinelibrary.wiley.com/doi/10.1029/2020JC017114 by Cochrane France, Wiley Online Library on [16/03/2023]. See the Terms and Conditions (https://onlinelibrary.wiley.com/terms-and-conditions) on Wiley Online Library for rules of use; OA articles are governed by the applicable Creative Commons License

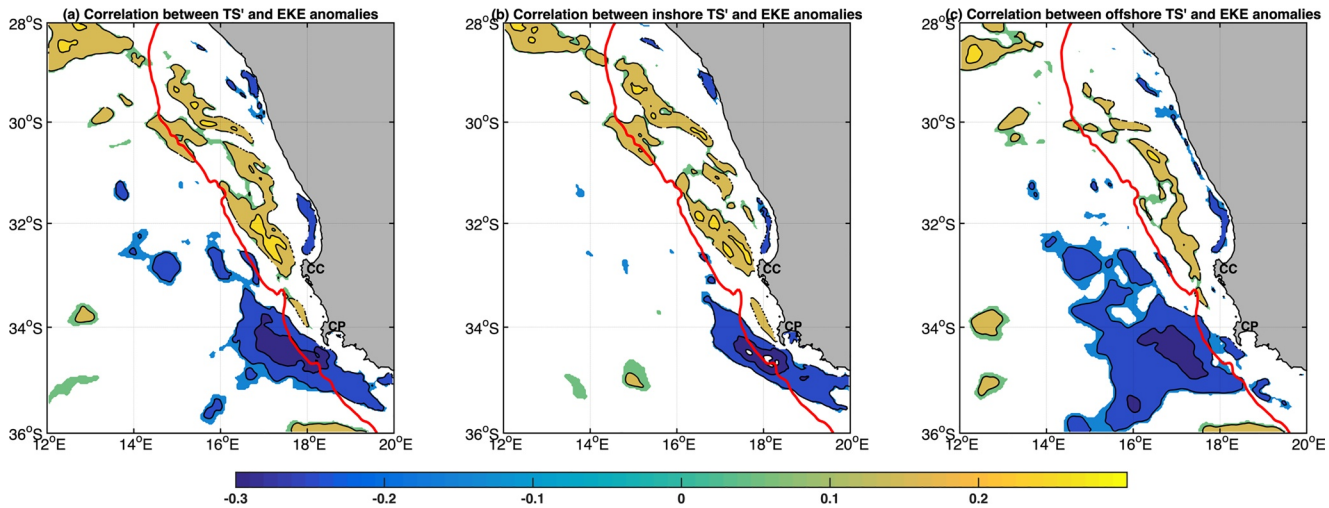

Figure 16. Correlation maps of EKE and transport success anomalies for different subgroups of particles. (a) All successful particles (TS′). (b) The subgroup made of all successful inshore particles (TSI′). (c) The subgroup made of all successful offshore particles (TSO′). The 500-m isobath separating the inshore and offshore region is superimposed (solid red). Only the significant correlations at a 95% confidence level have been reported.

of Agulhas rings that pass near the SARP line. A total of 107 of such eddies were identified in an area situated south-west of Cape Point, also known in the literature as the Cape Cauldron (Boebel et al., 2003). This number was further reduced to 48 by only considering rings that followed the northern route into the South Atlantic (Dencausse et al., 2010), that is, the route that passes nearby the south-east Atlantic shelf. The trajectory of the 48 rings is shown in Figure 15d. To focus on the rings that might had an impact on the trajectories of the particles, only rings with a distance between the eddy center and the 3,000-m isobath to be $<1.5 \times R_{eddy}$ were considered. Only 18 rings (black trajectories in Figure 15d) were found to match the criteria, and influenced the coastal ocean circulation for a total of 177 days with eight influencing the inner-shelf for 36 days Table 3 resumes the influence of each of these 18 offshore rings on TSO′ only. Due to their brevity and infrequent interaction with the shelf edge, these rings had minimal effect inshore transport success anomaly TSI'.

Not all rings had an impact on TSO′, their level of impact is influenced mainly by their closeness to the SARP line. 28% of the Agulhas ring interactions resulted in positive offshore transport success anomalies, while the vast majority (72%) resulted in negative transport success anomalies. In addition, only nine of these interactions coincide with a standardized TSO′ > 0.4. In January 2000, an Agulhas ring passed closer to the 3,000-m isobath but far south of the SARP line (Figure 18, top), hence it had minimal impact on offshore transport of particles and transport success. In contrast, during January 2002, an Agulhas ring was located west, near the SARP line entrained most of the particles released on the outer shelf away from the shelf (Figure 18, bottom). This offshore transport prevented any early age northward transport and, therefore, reducing their chance to reach St Helena Bay.

6. Discussion and Conclusions

In the southern Benguela upwelling system (SBUS), variability in the annual recruitment of small pelagic fish has long been a significant concern to fisheries oceanographers. To be transported to a suitable nursery area is one of the factors required for the survival of fish larvae, and this study was aimed at relating anomalous transport success events to local physical processes such as (a) wind surface forcing (Ekman transport, Benguela Jet, poleward current) and (b) mesoscale dynamics. The inter-annual variability in physical transport processes was investigated using a 3-km high-resolution simulation forced with 6-hourly atmospheric CFSR data provided for 20 years (1992–2011). The approach consisted of computing transport success anomalies and characterizing the local wind-driven ocean circulation and mesoscale turbulence. The results showed that competing physical processes impact the alongshore connectivity in the Southern Benguela, leading to strong inter-annual variability of the transport success time series.

21699291, 2022, 3, Downloaded from https://agupubs.onlinelibrary.wiley.com/doi/10.1029/2020JC017114 by Cochrane France, Wiley Online Library on [16/03/2023]. See the Terms and Conditions (https://onlinelibrary.wiley.com/terms-and-conditions) on Wiley Online Library for rules of use; OA articles are governed by the applicable Creative Commons License

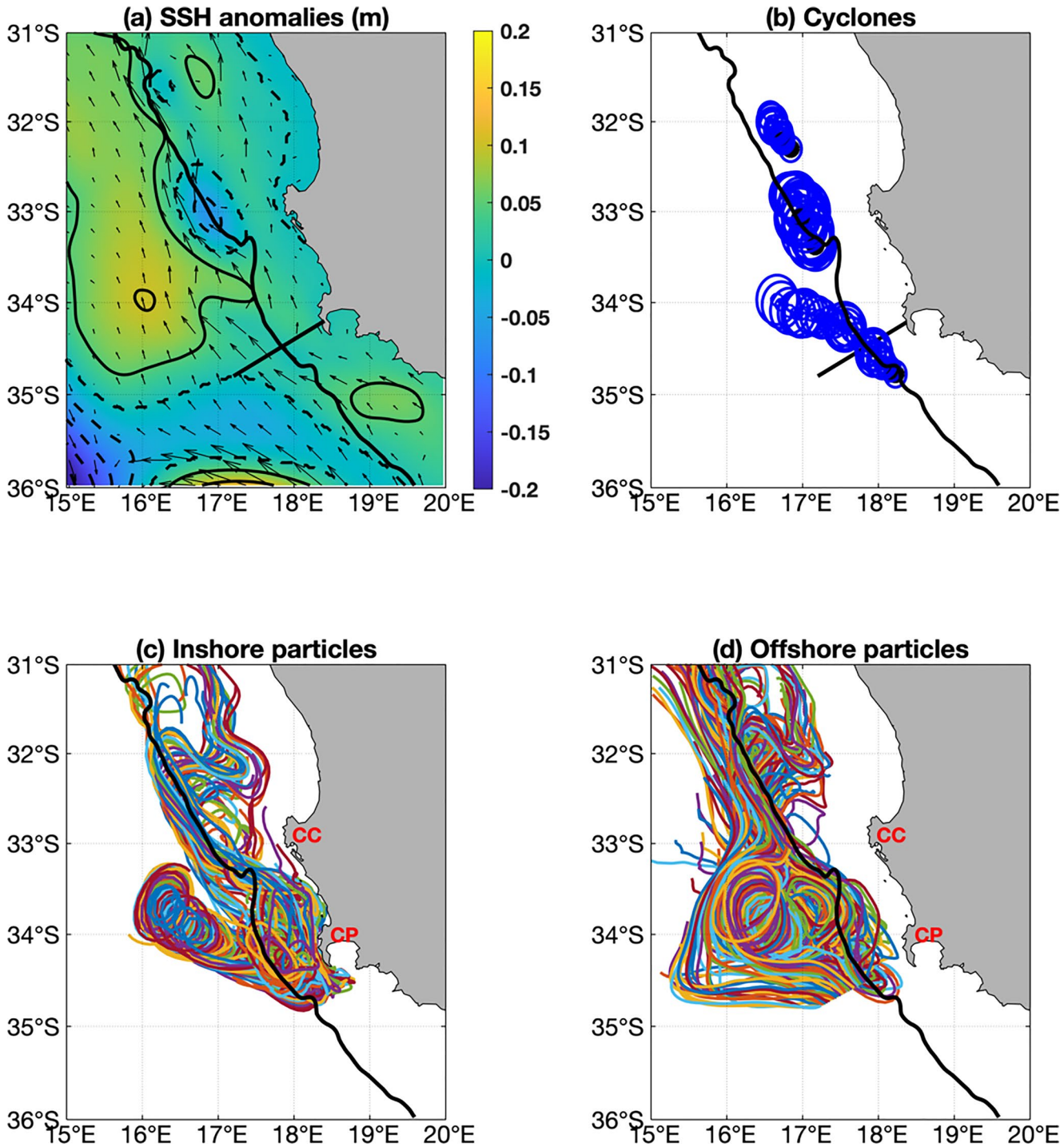

Figure 17. (a) April 1992 monthly average of SSH anomalies (m) and surface current velocities(vectors). (b) Daily successive contours delineating the size and position of three (3) cyclonic eddies (circles) detected between Cape Point and Cape Columbine in April 1992. (c) Trajectories of randomly chosen inshore particles. (d) Same as (c) for randomly chosen offshore particles.

During most of the years, particles successfully traveling to St Helena Bay predominantly originate from the inner-shelf and use the Benguela Jet, the strong alongshore surface current flowing northward over the 200–500 m isobaths, as their main conveyor (Ragoasha et al., 2019). Therefore, not surprisingly, the variability in the transport success of the inner-shelf subgroup of particles was strongly related to the jet's variability itself, and to processes capable of removing particles from the jet, mainly the variability of the offshore surface

21699291, 2022, 3, Downloaded from https://agupubs.onlinelibrary.wiley.com/doi/10.1029/2020JC017114 by Cochrane France, Wiley Online Library on [16/03/2023]. See the Terms and Conditions (https://onlinelibrary.wiley.com/terms-and-conditions) on Wiley Online Library for rules of use; OA articles are governed by the applicable Creative Commons License

Table 3
Census of 18 Agulhas Rings (Rows) Spotted in the Vicinity the 3,000-m Isobath and the SARP Line in the R3KM Simulation. From Left to Right, Columns Correspond to: The Year and Month the Eddy was Detected; The Number of Days the Eddy Stayed in the Vicinity of the SARP Line; The Average Distance of the Eddy Center to the SARP Line Over the Number of Days Spent Interacting With the 3,000-m Isobath Normalized by the Average Eddy Radius; TSO'_m

Years	Months	Days spent nearby the shelf	$\frac{d_{shelf-eddy}}{R_{eddy}}$	TSO′
1992	January	12	0.92	−0.40
1993	March	10	0.97	0.41
1993	September*	3	0.90	0.45
1994	October	20	1.10	0.35
1994	November	7	1.31	−0.17
1996	November	10	1.15	−0.94
1997	April	1	1.14	−0.19
2000	January*	5	0.75	0.60
2000	February*	7	0.78	−0.15
2001	January	13	1.22	−0.12
2001	December*	7	0.92	−0.22
2002	January	5	1.19	−0.85
2004	November*	19	0.82	−0.07
2004	December*	7	1.16	−0.82
2008	September*	8	0.72	−0.35
2008	October*	31	0.71	−0.56
2008	November	9	1.12	−0.75
2011	October	3	0.97	−0.03

Note. (*) denotes instances when the ring had an interaction with the shelf edge (500 m isobath).

Ekman transport. During the upwelling season, negative events of transport success are caused by the offshore removal of inshore particles through wind-driven offshore Ekman transport. Interestingly, these negative events tend to also coincide with bursts of the inner-shelf poleward counter-current. In fact, the Benguela Jet and the inner-shelf poleward counter-current are both wind-driven and dynamically connected to each other, the poleward counter-current causing the Benguela jet to shift offshore (Ragoasha et al., 2019). Bursts of the poleward counter-current tend to occur during periods of strong upwelling favorable winds ($r = +0.50$, $p < 0.005$), which explains why, in summer, a negative correlation is found between the Benguela Jet and the coastal poleward counter-current ($r = -0.8$, $p < 0.005$). In addition, there is a summer negative correlation between upwelling favorable winds and the Benguela Jet ($r = -0.52$, $p < 0.005$).

Particles released on the outer shelf also contribute to the total transport success all year round. Although their contribution is in average less than the one of the inshore particles, their role becomes as important during winter (Ragoasha et al., 2019). Their route to St Helena Bay takes longer and is considered to be more hazardous, because they are more likely to be influenced by the sustained offshore mesoscale eddy field, and therefore to have chaotic trajectories. Nevertheless, interestingly, some offshore particles that get transported further into the open ocean do manage to come back inshore and contribute to positive offshore transport success. Considering the inter-annual variability of total transport anomaly, our results show that their contribution is significant (Figure 13), and on the same order of magnitude of the one of the inshore particles $\left(\overline{TSI'^2} = \overline{TSO'^2}\right)$. They even are the most important contributors to the largest positive total transport success anomalies. Interestingly, the TSI′ and TSO′ time series are weakly but positively correlated ($r = 0.4$, $p < 0.05$), highlighting some similarities, but also differences between physical processes impacting the inner and outer shelf. However, extreme events ($|TS'_m| > 1$) appear to be the consequence of environmental conditions impacting similarly, in a favorable or unfavorable way, both inshore and offshore subgroups of particles ($r = 0.72$, $p < 0.05$).

Although multiple physical processes impact the along-shore connectivity in the southern Benguela, extended periods of negative and positive anomalies in the 20 years time series of TS′ (Figure 7) could be explained by a common combination of three physical drivers. The positive events of 1992–1993 and 1998–2001 are associated with stronger than average Benguela Jet, weaker upwelling favorable winds, and fewer occurrence of the coastal poleward counter-current, whereas the negative periods of 1994–1997 and 2011 are associated with the exact opposite combination. These results may question the predictability of the connectivity, and therefore its relation to the local inter-annual wind variability directly attributed to large-scale climate modes such as El Niño-Southern Oscillation (ENSO) and Southern Annular Mode (SAM; Dufois et al., 2012; Hall & Visbeck, 2002; Marshall, 2003; Risien et al., 2004; Tim et al., 2015). This impact was found to be small (not shown). However, a significant negative relationship ($r = -0.62$, $p < 0.005$) was found between summer wind anomalies and ENSO, suggesting that stronger south easterlies may be expected during La Niña years (Colberg et al., 2004) and contribute to enhanced offshore loss of inshore particles. However, no significant correlation was found between the Benguela Jet, the poleward current, the offshore EKE, and ENSO.

The short-time scale variability of the transport success time series may be induced by a random combination of the multiple physical drivers, including the direct impact of the offshore mesoscale eddy field, which by nature is itself also unpredictable. Year 1998 offers an illustration where an anomalously strong Benguela Jet counter-acts the negative effect on transport success induced by high offshore Ekman transport. Coherent mesoscale eddies in the vicinity of the shelf edge can also induce cross-shore advection of particles. The nature of this advection will

21699291, 2022, 3, Downloaded from https://agupubs.onlinelibrary.wiley.com/doi/10.1029/2020JC017114 by Cochrane France, Wiley Online Library on [16/03/2023]. See the Terms and Conditions (https://onlinelibrary.wiley.com/terms-and-conditions) on Wiley Online Library for rules of use; OA articles are governed by the applicable Creative Commons License

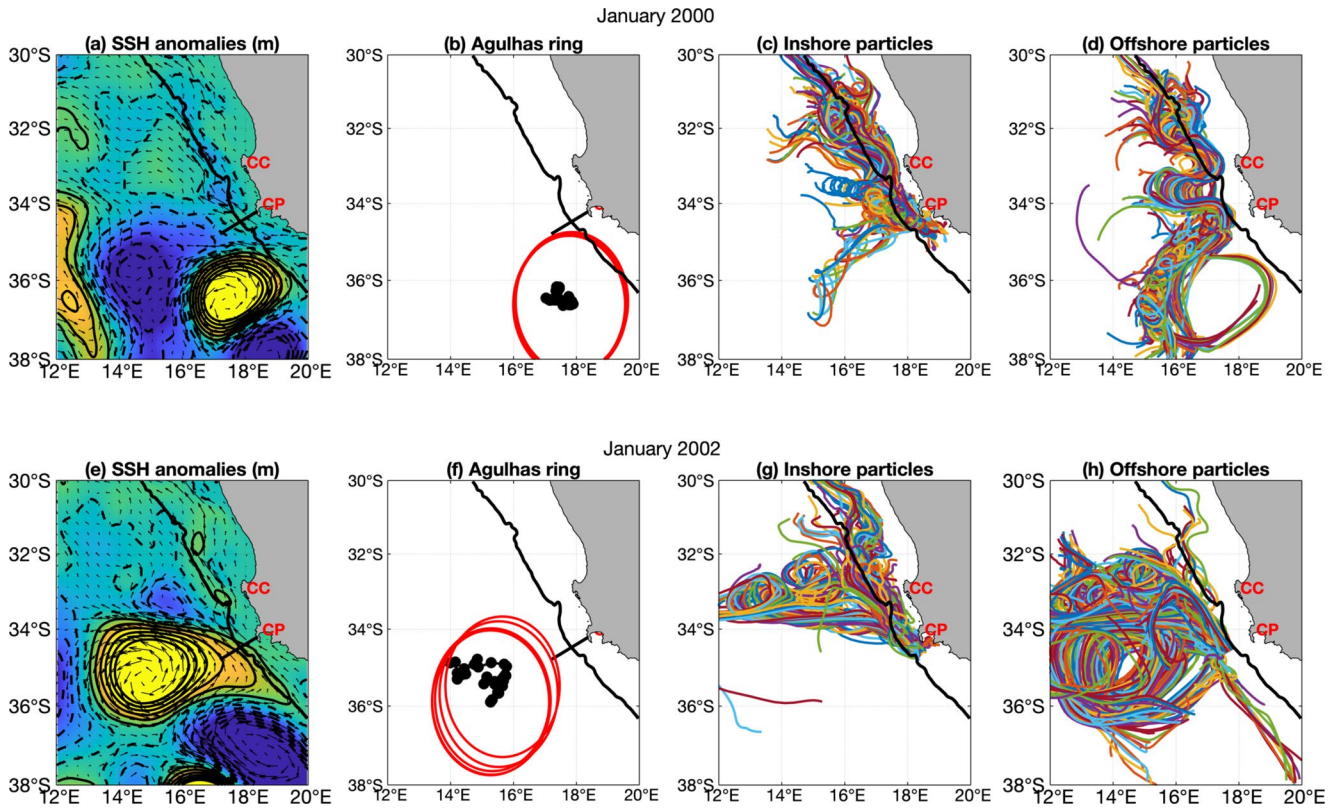

Figure 18. Two scenarios of an Agulhas ring passing nearby the 3,000-m isobath. (top): January 2000. The ring is located south of the SARP line and has little impact on the off-shore transport of particles. (bottom): January 2002. The ring is located west of the SARP line and drives a large amount of the shelf-edge particles off-shore. (a)–(e) Monthly mean of the SSH anomaly with geostrophic surface currents superimposed (vectors). (b)–(f) Trajectory of the ring center while it interacts with the shelf edge (dots). Red circles are drawn from the eddy center with a radius equal to $1.5 \times R_{eddy}$. (c)–(g): Random trajectories of the inshore subgroup of particles. (d)–(h) Random trajectories of the offshore subgroup of particles. The 500-m isobath is superimposed on every map (solid black).

however be very sensitive to the polarities, sizes, and intensities of the nearby eddies. One can expect a strong variability both temporally and spatially along-shore.

Nevertheless, our analysis shows some kind of pattern for the shelf-edge cyclonic eddies that result from the inshore instabilities of the upwelling density front. Because they propagate along the shelf edge, they contribute to keeping inshore particles on the shelf and to entrain offshore particles inshore. The impact of anticyclones may be more challenging to predict. Our study reveals that they can have huge effects at the SARP line, where the early age northward along-shore transport is crucial for successful connectivity.

It is important to note that the presented results may be sensitive to model resolution. The presence of intense vertical velocities triggered by submesoscale frontal turbulence (Capet et al., 2008) could lead to particles trajectories with larger depth variations, which could in turn modify their dispersion if there is strong vertical shear of the horizontal flow. The ability of the model to adequately capture the Agulhas leakage and its associated mesoscale turbulence, is also essential. This leakage can take place through large coherent anticyclonic eddies, but smaller size vortices and filaments also play a role. Overestimation of the Agulhas leakage in coarse resolution models, as well as the misrepresentation of the turbulent features and their interactions with the southern Benguela shelf are likely to lead to unrealistic estimates of transport success.

Moreover, underestimation of the abundance of small cyclonic shelf eddies in such models could also lead to the unrealistic offshore removal of inshore particles, as well as an underestimation of the number of offshore particles managing to get advected toward the inshore shelf. Although we did not investigate the physical processes related to the generation of these shelf cyclonic eddies, our results have shown that they participate in maintaining particles over the shelf.

21699291, 2022, 3, Downloaded from https://agupubs.onlinelibrary.wiley.com/doi/10.1029/2020JC017114 by Cochrane France, Wiley Online Library on [16/03/2023]. See the Terms and Conditions (https://onlinelibrary.wiley.com/terms-and-conditions) on Wiley Online Library for rules of use; OA articles are governed by the applicable Creative Commons License

This study investigated how physical processes can impact transport success between Cape Point and St Helena Bay. These findings could now be used to shed some light on the processes governing small pelagic fish recruitment variability in the SBUS. However, studying the retention of particles in St Helena Bay, after their arrival, is also another important process to consider since the retention of larvae in a suitable habitat is also one of the key factors proposed by Bakun's fundamental triad processes (Bakun, 1996). More realistic studies would then require the incorporation of anchovy population dynamics that include biological properties such as egg density, diel vertical motion, mortality due to starvation and predation (Huggett et al., 2003; Koné et al., 2013; Mullon et al., 2003; Parada et al., 2003, 2008).

Appendix A

A1. Detection of Across-Shelf Displacements

Successful particles are divided into subgroups whether they experience offshore displacements. In the absence of diabatic processes, shelf particles tend to be advected along the isobaths to conserve their potential vorticity (Le Paih et al., 2020). Lagrangian across-shelf displacements are therefore quantified by recording the Lagrangian changes of the isobaths located below the particles. The maximum off-shore displacement (Δx) of each successful particle during its journey to St Helena Bay is then computed as the across-shore distance separating two isobaths, the isobath at the particle's position at instant t and the initial isobath above which it has been released.

$$\Delta x_i(t) = x_i(t) - x_i(t = 0) \tag{A1}$$

where i is the subindex of the individual Lagrangian particle, x an abscissa representing the cross-shore position of a particle relative to the 500 m isobath, and t the age of a particle. When $\|\Delta_x\| > 50$ km and corresponds to offshore displacement, the particle is considered to have experienced a significant offshore displacement. Therefore, it is assigned an offshore subgroup. Characteristics of the four subgroups are resumed in Table 1.

Data Availability Statement

The 3-km ROMS model configuration of the southern Benguela and Pyticles Lagrangian data used in this study is archived on Zenodo: available for download at https://doi.org/10.5281/zenodo.4281339.

Acknowledgments
The authors acknowledge the funding of N. Ragoasha's PhD by the South-African National Research Foundation (NRF, South Africa) and the French Institute for Research and Sustainable Development (IRD, France). This study was also supported by the French national program LEFE/INSU under the project's name Benguela Upwelling Innershelf Circulation (BUIC). This study was granted access to the HPC resources of [TGCC/CINES/IDRIS] under the allocation 2017-[DARI no. A0020107443] attributed by GENCI (Grand Equipement National de Calcul Intensif).

References

Bakun, A. (1996). *Patterns in the ocean: Ocean processes and marine population dynamics*. La Paz, Mexico: California Sea Grant, in cooperation with Centro de Investigaciones Biologicas del Noroeste.

Bang, N., & Andrews, W. (1974). Direct-current measurements of a shelf-edge frontal jet in southern benguela system. *Journal of Marine Research*, *32*(3), 405–417.

Beal, L. M., De Ruijter, W. P. M., Biastoch, A., Zahn, R., Cronin, M., Hermes, J., & Zinke, J. (2011). On the role of the agulhas system in ocean circulation and climate. *Nature*, *472*, 429–436. https://doi.org/10.1038/nature09983

Biastoch, A., Böning, C. W., Schwarzkopf, F. U., & Lutjeharms, J. R. E. (2009). Increase in Agulhas leakage due to poleward shift of Southern Hemisphere westerlies. *Nature*, *462*(7272), 495–498. https://doi.org/10.1038/nature08519

Blanke, B., Penven, P., Roy, C., Chang, N., & Kokoszka, F. (2009). Ocean variability over the agulhas bank and its dynamical connection with the southern benguela upwelling system. *Journal of Geophysical Research: Oceans*, *114*(C12). https://doi.org/10.1029/2009JC005358

Blanke, B., Speich, S., Bentamy, A., Roy, C., & Sow, B. (2005). Modeling the structure and variability of the southern Benguela upwelling using QuikSCAT wind forcing. *Journal of Geophysical Research: Oceans*, *110*(C7). https://doi.org/10.1029/2004jc002529

Boebel, O., Lutjeharms, J., Schmid, C., Zenk, W., Rossby, T., & Barron, C. (2003). The cape cauldron: A regime of turbulent inter-ocean exchange. *Deep Sea Research Part II: Topical Studies in Oceanography*, *50*(1), 57–86. https://doi.org/10.1016/S0967-0645(02)00379-X

Brown, P. C., & Hutchings, L. (1987). The development and decline of phytoplankton blooms in the southern Benguela upwelling system. 1. Drogue movements, hydrography and bloom development. *South African Journal of Marine Science*, *5*(1), 357–391. https://doi.org/10.2989/025776187784522801

Capet, X., McWilliams, J. C., Molemaker, M. J., & Shchepetkin, A. F. (2008). Mesoscale to submesoscale transition in the California Current System. Part II: Frontal processes. *Journal of Physical Oceanography*, *38*(1), 44–64. https://doi.org/10.1175/2007JPO3672.1

Colberg, F., Reason, C. J. C., & Rodgers, K. (2004). South Atlantic response to El Niño-Southern Oscillation induced climate variability in an ocean general circulation model. *Journal of Geophysical Research: Oceans*, *109*(C12). https://doi.org/10.1029/2004JC002301

de Ruijter, W. P. M., van Leeuwen, P. J., & Lutjeharms, J. R. E. (1999). Generation and evolution of natal pulses: Solitary meanders in the agulhas current. *Journal of Physical Oceanography*, *29*(12), 3043–3055. https://doi.org/10.1175/1520-0485(1999)029<3043:gaeonp>2.0.co;2

Dencausse, G., Arhan, M., & Speich, S. (2010). Routes of agulhas rings in the southeastern cape basin. *Deep Sea Research Part I: Oceanographic Research Papers*, *57*(11), 1406–1421. https://doi.org/10.1016/j.dsr.2010.07.008

Dufois, F., Penven, P., Peter Whittle, C., & Veitch, J. (2012). On the warm nearshore bias in Pathfinder monthly SST products over Eastern Boundary Upwelling Systems. *Ocean Modelling*, *47*, 113–118. https://doi.org/10.1016/j.ocemod.2012.01.007

21699291, 2022, 3, Downloaded from https://agupubs.onlinelibrary.wiley.com/doi/10.1029/2020JC017114 by Cochrane France, Wiley Online Library on [16/03/2023]. See the Terms and Conditions (https://onlinelibrary.wiley.com/terms-and-conditions) on Wiley Online Library for rules of use; OA articles are governed by the applicable Creative Commons License

Duncombe-Rae, C., Shillington, F., Agenbag, J., Taunton-Clark, J., & Gründlingh, M. (1992). An agulhas ring in the south atlantic ocean and its interaction with the benguela upwelling frontal system. *Deep Sea Research Part A. Oceanographic Research Papers*, *39*(11), 2009–2027. https://doi.org/10.1016/0198-0149(92)90011-H

Durgadoo, J. V., Loveday, B. R., Reason, C. J. C., Penven, P., & Biastoch, A. (2013). Agulhas leakage predominantly responds to the southern hemisphere westerlies. *Journal of Physical Oceanography*, *43*(10), 2113–2131. https://doi.org/10.1175/JPO-D-13-047.1

Fawcett, A. L., Pitcher, G., & Shillington, F. (2008). Nearshore currents on the southern Namaqua shelf of the Benguela upwelling system. *Continental Shelf Research*, *28*(8), 1026–1039. https://doi.org/10.1016/j.csr.2008.02.005

Fowler, J. L., & Boyd, A. J. (1998). Transport of anchovy and sardine eggs and larvae from the western agulhas bank to the west coast during the 1993/94 and 1994/95 spawning seasons. *South African Journal of Marine Science*, *19*(1), 181–195. https://doi.org/10.2989/025776198784127006

Garcia, H., Boyer, T., Locarnini, R., Baranova, O., Zweng, M., & Mishonov, A. V. (2018). *World ocean database 2018: User's manual (prerelease)* (Technical ed.). Silver Spring: NOAA.

Gordon, A. (1985). Indian-Atlantic transfer of thermohaline water at the Agulhas retroflection. *Science*, *227*, 1030–1033. https://doi.org/10.1126/science.227.4690.1030

Gula, J., Molemaker, M. J., & McWilliams, J. C. (2014). Submesoscale cold filaments in the Gulf Stream. *Journal of Physical Oceanography*, *44*(10), 2617–2643. https://doi.org/10.1175/JPO-D-14-0029.1

Hall, A., & Visbeck, M. (2002). Synchronous variability in the southern hemisphere atmosphere, sea ice, and ocean resulting from the annular mode. *Journal of Climate*, *15*(21), 3043–3057. https://doi.org/10.1175/1520-0442(2002)015<3043:svitsh>2.0.co;2

Hall, C., & Lutjeharms, J. (2011). Cyclonic eddies identified in the cape basin of the south atlantic ocean. *Journal of Marine Systems*, *85*, 1–10. https://doi.org/10.1016/j.jmarsys.2010.10.003

Halo, I., Penven, P., Backeberg, B., Ansorge, I., Shillington, F., & Roman, R. (2014). Mesoscale eddy variability in the southern extension of the east Madagascar current: Seasonal cycle, energy conversion terms, and eddy mean properties. *Journal of Geophysical Research: Oceans*, *119*(10), 7324–7356. https://doi.org/10.1002/2014JC009820

Hampton, I. (1996). Acoustic and egg-production estimates of South African anchovy biomass over a decade: Comparisons, accuracy, and utility. *ICES Journal of Marine Science*, *53*(2), 493–500. https://doi.org/10.1006/jmsc.1996.0071

Hardman-Mountford, N. J., Richardson, A. J., Agenbag, J. J., Hagen, E., Nykjaer, L., Shillington, F. A., & Villacastin, C. (2003). Ocean climate of the South East Atlantic observed from satellite data and wind models. *Progress in Oceanography*, *59*(2–3), 181–221. https://doi.org/10.1016/j.pocean.2003.10.001

Huggett, J., Fréon, P., Mullon, C., & Penven, P. (2003). Modelling the transport success of anchovy Engraulis encrasicolus eggs and larvae in the southern Benguela: The effect of spatio-temporal spawning patterns. *Marine Ecology Progress Series*, *250*(Linnaeus 1758), 247–262. https://doi.org/10.3354/meps250247

Hutchings, L. (1992). Fish harvesting in a variable, productive environment—Searching for rules or searching for exceptions? *South African Journal of Marine Science*, *12*(1), 297–318. https://doi.org/10.2989/02577619209504708

Hutchings, L., Barange, M., Bloomer, S. F., Boyd, A. J., Crawford, R. J. M., Huggett, J. A., et al. (1998). Multiple factors affecting South African anchovy recruitment in the spawning, transport and nursery areas. *South African Journal of Marine Science*, *19*(1), 211–225. https://doi.org/10.2989/025776198784126908

Illig, S., Bachèlery, M.-L., & Cadier, E. (2018). Subseasonal coastal-trapped wave propagations in the southeastern pacific and atlantic oceans: 2. Wave characteristics and connection with the equatorial variability. *Journal of Geophysical Research: Oceans*, *123*(6), 3942–3961. https://doi.org/10.1029/2017JC013540

Illig, S., Cadier, E., Bachelery, M.-L., & Kersalé, M. (2018). Subseasonal coastal-trapped wave propagations in the southeastern Pacific and Atlantic Oceans: 1. A new approach to estimate wave amplitude. *Journal of Geophysical Research: Oceans*, *123*, 3915–3941. https://doi.org/10.1029/2017JC013539

Koné, V., Lett, C., & Fréon, P. (2013). Modelling the effect of food availability on recruitment success of cape anchovy ichthyoplankton in the southern benguela upwelling system. *African Journal of Marine Science*, *35*(2), 151–161. https://doi.org/10.2989/1814232X.2013.796893

Le Paih, N., Hattermann, T., Boebel, O., Kanzow, T., Lüpkes, C., Rohardt, G., et al. (2020). Coherent seasonal acceleration of the Weddell sea boundary current system driven by upstream winds. *Journal of Geophysical Research: Oceans*, *125*(10), e2020JC016316. https://doi.org/10.1029/2020JC016316

Loveday, B. R., Durgadoo, J. V., Reason, C. J., Biastoch, A., & Penven, P. (2014). Decoupling of the Agulhas leakage from the Agulhas Current. *Journal of Physical Oceanography*, 140411151744003. https://doi.org/10.1175/JPO-D-13-093.1

Marshall, G. J. (2003). Trends in the southern annular mode from observations and reanalyses. *Journal of Climate*, *16*(24), 4134–4143. https://doi.org/10.1175/1520-0442(2003)016<4134:titsam>2.0.co;2

Mason, E., Molemaker, J., Shchepetkin, A. F., Colas, F., McWilliams, J. C., & SangrÃ, P. (2010). Procedures for offline grid nesting in regional ocean models. *Ocean Modelling*, *35*(1), 1–15. https://doi.org/10.1016/j.ocemod.2010.05.007

Mullon, C., Fréon, P., Parada, C., Van Der Lingen, C., & Huggett, J. (2003). From particles to individuals: Modelling the early stages of anchovy (Engraulis capensis/encrasicolus) in the southern Benguela. *Fisheries Oceanography*, *12*(4–5), 396–406. https://doi.org/10.1046/j.1365-2419.2003.00240.x

Nelson, G. (1989). Poleward motion in the benguela area. In *Poleward flows along eastern ocean boundaries* (pp. 110–130). American Geophysical Union. https://doi.org/10.1007/978-1-4613-8963-7_10

Painting, S. J., Hutchings, L., Hugget, J. A., Korrûbel, J. L., Richardson, A. J., & Verheye, H. M. (1998). Environmental and biological monitoring for forecasting anchovy recruitment in the southern benguela upwelling region. *Fisheries Oceanography*, *7*(34), 364–374. https://doi.org/10.1046/j.1365-2419.1998.00086.x

Parada, C., Mullon, C., Roy, C., Fréon, P., Hutchings, L., & Van Der Lingen, C. D. (2008). Does vertical migratory behaviour retain fish larvae onshore in upwelling ecosystems? A modelling study of anchovy in the southern Benguela. *African Journal of Marine Science*, *30*(3), 437–452. https://doi.org/10.2989/AJMS.2008.30.3.1.635

Parada, C., Van Der Lingen, C. D., Mullon, C., & Penven, P. (2003). Modelling the effect of buoyancy on the transport of anchovy (Engraulis capensis) eggs from spawning to nursery grounds in the southern Benguela: An IBM approach. *Fisheries Oceanography*, *12*(3), 170–184. https://doi.org/10.1046/j.1365-2419.2003.00235.x

Parrish, R. H., Bakun, A., Husby, D. M., & Nelson, C. S. (1983). *Comparative climatology of selected environmental processes in relation to eastern boundary current pelagic fish reproduction*. FAO Fisheries Report (FAO).

Penven, P., Lutjeharms, J. R. E., Marchesiello, P., Roy, C., & Weeks, S. J. (2000). Generation of cyclonic eddies by the agulhas current in the lee of the agulhas bank. *Geophysical Research Letters*, *28*(6), 1055–1058. https://doi.org/10.1029/2000GL011760

Ragoasha, N., Herbette, S., Cambon, G., Veitch, J., Reason, C., & Roy, C. (2019). Lagrangian pathways in the southern benguela upwelling system. *Journal of Marine Systems*, *195*, 50–66. https://doi.org/10.1016/j.jmarsys.2019.03.008

21699291, 2022, 3, Downloaded from https://agupubs.onlinelibrary.wiley.com/doi/10.1029/2020JC017114 by Cochrane France, Wiley Online Library on [16/03/2023]. See the Terms and Conditions (https://onlinelibrary.wiley.com/terms-and-conditions) on Wiley Online Library for rules of use; OA articles are governed by the applicable Creative Commons License

Risien, C. M., Reason, C. J. C., Shillington, F. A., & Chelton, D. B. (2004). Variability in satellite winds over the benguela upwelling system during 1999-2000. *Journal of Geophysical Research: Oceans*, *109*(C3). https://doi.org/10.1029/2003JC001880

Rubio, A., Blanke, B., Speich, S., Grima, N., & Roy, C. (2009). Mesoscale eddy activity in the southern Benguela upwelling system from satellite altimetry and model data. *Progress in Oceanography*, *83*(1–4), 288–295. https://doi.org/10.1016/j.pocean.2009.07.029

Saha, e. a., & Suranjana. (2010). The ncep climate forecast system reanalysis. *The Bulletin of the American Meteorological Society*, *91*(8), 1015–1057. https://doi.org/10.1175/2010BAMS3001.1

Shannon, L., Nelson, G., Crawdord, R., & Boyd, A. (1996). Possible impacts of environmental change on pelagic fish recruitment: Modelling anchovy transport by advective processes in the southern Benguela. *Global Change Biology*, *2*(5), 407–420. https://doi.org/10.1111/j.1365-2486.1996.tb00091.x

Shelton, P. A., & Hutchings, L. (1982). Transport of anchovy, *Engraulis capensis* Gilchrist, eggs and early larvae by a frontal jet current. *Journal du Conseil*, *40*(2), 185–198. https://doi.org/10.1093/icesjms/40.2.185

Shillington, F. A. (1998). The benguela upwelling system off southwestern africa, the sea, vol. 11. In A. R.Robinson & K. H.Brink (Eds.), *The global coastal ocean, regional studies and syntheses* (pp. 583–604). New York: Wiley.

Tim, N., Zorita, E., & Hünicke, B. (2015). Decadal variability and trends of the Benguela upwelling system as simulated in a high-resolution ocean simulation. *Ocean Science*, *11*(3), 483–502. https://doi.org/10.5194/os-11-483-2015

van der Lingen, C., Coetzee, J., & Hutchings, L. (2002). Temporal shifts in the spatial distribution of anchovy spawners and their eggs in the southern benguela: Implications for recruitment. *Globec Report*, *16*, 46–48.

van der Lingen, C., & Huggett, J. (2003). *The role of ichthyoplankton surveys in recruitment research and management of South African anchovy and sardine*.

van Sebille, E., Barron, C. N., Biastoch, A., van Leeuwen, P. J., Vossepoel, F. C., & de Ruijter, W. P. M. (2009). Relating agulhas leakage to the agulhas current retroflection location. *Ocean Science*, *5*(4), 511–521. https://www.ocean-sci.net/5/511/2009/

Veitch, J., Florenchie, P., & Shillington, F. (2006). Seasonal and interannual fluctuations of the Angola-Benguela Frontal Zone (ABFZ) using 4.5 km resolution satellite imagery from 1982 to 1999. *The International Journal of Remote Sensing*, *27*, 987–998. https://doi.org/10.1080/01431160500127914

Veitch, J., Hermes, J., Lamont, T., Penven, P., & Dufois, F. (2017). Shelf-edge jet currents in the southern Benguela: A modelling approach. *Journal of Marine Systems*. https://doi.org/10.1016/j.jmarsys.2017.09.003

Veitch, J., & Penven, P. (2017). The role of the Agulhas in the Benguela Current system: A numerical modeling approach. *Journal of Geophysical Research*, *122*(4), 3375–3393. https://doi.org/10.1002/2016JC012247

Veitch, J., Penven, P., & Shillington, F. (2009). The Benguela: A laboratory for comparative modeling studies. *Progress in Oceanography*, *83*(1–4), 296–302. https://doi.org/10.1016/j.pocean.2009.07.008

Vianello, P., Herbette, S., Ternon, J.-F., Demarcq, H., & Roberts, M. J. (2020). Observation of a mesoscale eddy dipole on the northern Madagascar ridge: Consequences for the circulation and hydrography in the vicinity of a seamount. *Deep Sea Research Part II: Topical Studies in Oceanography*, *176*, 104815. https://doi.org/10.1016/j.dsr2.2020.104815

21699291, 2022, 3, Downloaded from https://agupubs.onlinelibrary.wiley.com/doi/10.1029/2020JC017114 by Cochrane France, Wiley Online Library on [16/03/2023]. See the Terms and Conditions (https://onlinelibrary.wiley.com/terms-and-conditions) on Wiley Online Library for rules of use; OA articles are governed by the applicable Creative Commons License